1 **A high-resolution time-of-flight chemical ionization mass spectrometer**

2 **utilizing hydronium ions (H_3O^+ ToF-CIMS) for measurements of**

3 **volatile organic compounds in the atmosphere**

4 Bin Yuan[1,2], Abigail Koss[1,2,3], Carsten Warneke[1,2], Jessica B. Gilman[1,2], Brian M.

5 Lerner[1,2], Harald Stark[2,3,4], Joost A. de Gouw[1,2,3]

6 *1. NOAA Earth System Research Laboratory (ESRL), Chemical Sciences Division, Boulder, CO,*

7 *USA*

8 *2. Cooperative Institute for Research in Environmental Sciences, University of Colorado at*

9 *Boulder, Boulder, CO, USA*

10 *3. Department of Chemistry and Biochemistry, University of Colorado at Boulder, CO, USA*

11 *4. Aerodyne Research Inc., Billerica, MA 01821, USA*

13 Correspondence to Bin Yuan (bin.yuan@noaa.gov)

15 **Manuscript prepared for *Atmospheric Measurement Techniques***

Abstract

Proton transfer reactions between hydronium ions (H_3O^+) and volatile organic compounds (VOCs) provide a fast and high sensitive measurement technique for VOCs, leading to extensive use of proton-transfer-reaction mass spectrometry (PTR-MS) in atmospheric research. Based on the same ionization approach, we describe the development of a high-resolution (HR) time of flight chemical ionization mass spectrometer (ToF-CIMS) utilizing H_3O^+ as the reagent ions. The new H_3O^+ ToF-CIMS has sensitivities of 100-1000 cps/ppb (ion counts per second per part-per-billion mixing ratio of VOC) and detection limits of 20-600 ppt at 3σ for a 1-second integration time for simultaneous measurements of many VOC species of atmospheric relevance. Compared with similar instruments with quadrupole mass spectrometer, e.g. proton-transfer-reaction mass spectrometers, the ToF analyzer with mass resolution ($m/\Delta m$) of up to 6000 not only increases measurement frequency of the instrument, but also expands the number of measurable species. The humidity dependence of the instrument was characterized for various VOC species and the behaviors for different species can be explained by compound-specific properties that affect the ion chemistry. The new H_3O^+ ToF-CIMS was successfully deployed on the NOAA WP-3D research aircraft for the SONGNEX campaign in spring of 2015. The measured mixing ratios of several aromatics from the H_3O^+ ToF-CIMS agreed within ±10% with independent gas chromatography (GC) measurements from whole air samples. Initial results from the SONGNEX measurements demonstrate that the H_3O^+ ToF-CIMS dataset will be valuable for the identification and characterization of emissions from various sources, investigation of secondary formation of many photochemical organic products and therefore the chemical evolution of gas-phase organic carbon in the atmosphere.

1.   Introduction

43   Volatile organic compounds (VOCs) are ubiquitous in the atmosphere. The

44   oxidation of VOCs contributes to formation of ozone (Atkinson, 2000) and secondary

45   organic aerosol (SOA) (Hallquist et al., 2009). Accurate measurements of VOCs in the

46   atmosphere are essential to understand their sources, chemical transformations and hence

47   their effects on ozone and SOA formation (Isaksen et al., 2009). Measurements of VOCs

48   require techniques with high time resolution to effectively capture their high variability in

49   the atmosphere, especially for measurements performed on mobile platforms.

50   Proton transfer reaction mass spectrometry (PTR-MS) has been an important

51   scientific tool for VOC measurements, associated with high sensitivity and fast time

52   response (de Gouw and Warneke, 2007;Lindinger et al., 1998;Blake et al., 2009). The

53   first generation of PTR-MS instruments used quadrupole mass spectrometers (QMS) for

54   the detection of reagent and product ions. For atmospheric measurements, PTR-QMS

55   instruments are usually used in selected-ion mode, in which the mass filter steps through

56   several pre-selected masses consecutively each with a dwell time of 0.1-1 s (Warneke et

57   al., 2015). The measurement frequency for each species is thus determined by the total

58   cycle length, which is usually on the order of several seconds to 1 minute dependent on

59   user settings. The datasets produced from PTR-QMS are usually disjunct and the

60   information for masses beyond the selected ones is not available. The time resolution of

61   PTR-QMS is generally sufficient for ground-based measurements targeting VOC mixing

62   ratios, but not ideal for aircraft measurements or eddy covariance flux measurements of

63   more than a few species. In recent years, other mass analyzer, e.g. ion traps (Warneke et

64   al., 2005;Mielke et al., 2008;Steeghs et al., 2007) and time of flight (ToF) mass

65   spectrometers (Blake et al., 2004;Ennis et al., 2005;Tanimoto et al., 2007), were used in

66   PTR-MS to overcome some of these inherent drawbacks in PTR-QMS.

67   PTR-MS instruments that use time-of flight mass spectrometers (PTR-TOF) were

68   made commercially available in 2009 by Ionicon Analytik (Jordan et al., 2009). The

69   Ionicon PTR-TOF, equipped with Tofwerk orthogonal acceleration reflectron TOF-MS

70   (HTOF), had both much higher sensitivities (10-50 cps/ppbv) and better mass resolution

71   (m/Δm=~6000) than earlier PTR-TOF instruments (<5 cps/ppbv and m/Δm=100-1200)

72   (Jordan et al., 2009). Recently, a newer version of the Ionicon PTR-TOF equipped with a

73   quadrupole ion guide (PTR-QiTOF) was developed and is more sensitive (by a factor of

74   ~25) than the previous version of Ionicon PTR-TOF that uses an electrostatic ion lens

75   system (Sulzer et al., 2014). The performance of these PTR-TOF instruments surpasses

76   those of PTR-QMS in several ways due to the ability of the ToF to obtain whole mass

77   spectra and their high mass resolution. The high mass resolution of the ToF analyzer

78   facilitates separation of isobaric isomers (Graus et al., 2010;Sulzer et al., 2014), which

79   increases the number of measurable VOC species and reduces the possible chemical

80   interferences (Warneke et al., 2015). PTR-TOF has been used successfully in several

81   field campaigns at ground sites to measure concentrations and fluxes of a large suite of

82   VOC species (Park et al., 2013;Müller et al., 2010;Kaser et al., 2013;Holzinger et al.,

83   2013). Recently, an aircraft-deployable PTR-TOF with mass resolution up to ~1000 was

84   developed and successfully deployed on the NASA P-3B research aircraft during the

85   DISCOVER-AQ campaign (Müller et al., 2014a). The deployment of this PTR-TOF has

86   demonstrated many advantages over PTR-QMS for aircraft measurements, such as much

87   higher time resolution and hence better spatial resolution, and separation of several

88   isobaric masses in the lower mass ranges (Müller et al., 2014a).

89   In this study, a high-resolution ToF-CIMS utilizing hydronium ions (H_3O^+) similarly

90   to PTR-MS was developed based on the commercial Aerodyne ToF-CIMS (Lee et al.,

91   2014). This instrument contains two quadrupole ion guides to transport ions from the drift

92   tube reaction region to the time-of-flight mass analyzer. The quadrupole ion guides, as

93   demonstrated in the PTR-QiTOF recently (Sulzer et al., 2014), provide better

94   transmission efficiency for the reagent and product ions than the conventional ion lens

95   system. The new instrument was deployed onboard the NOAA WP-3D research aircraft

96   during the SONGNEX campaign in spring of 2015. Here, we will present development

97   and characterization of the instrument and its performance during the SONGNEX

98   campaign.

99   2. H_3O^+ TOF-CIMS instrument description

100   A commercial Aerodyne chemical ionization mass spectrometer (CIMS) (Lee et al.,

101   2014) was used to construct the airborne H_3O^+ ToF-CIMS (Figure 1). Briefly, the

102   Aerodyne ToF-CIMS consists of (1) an ion-molecule reaction (IMR) chamber, (2) a

103   small segmented radio frequency (RF) only quadrupole ion guide that is used as

104   collisional dissociation chamber (SSQ), (3) a second big segmented RF-only quadrupole

105   (BSQ), (4) a series of DC optics that further focus and accelerate the primary beam (PB),

106   and (5) a high-resolution ToF detector (HTOF, Tofwerk AG, Switzerland) (Bertram et

107   al., 2011). In the new H_3O^+ ToF-CIMS, the IMR chamber was replaced by a drift tube

108   (Figure 1), which provides a homogenous and controllable electric field for ion-molecule

109   reactions. The drift tube is comprised of stainless steel rings separated by Teflon rings for

110   both vacuum sealing and electronic insulation (de Gouw and Warneke, 2007). A hollow

111   cathode discharge ion source was connected in front of the drift tube to produce high

112   purity hydronium ions by introducing a flow of 5 mL min^{-1} of water vapor. The detailed

113   description for both drift tube and ion source can be found in previous review papers (de

114   Gouw and Warneke, 2007;Blake et al., 2009). In addition to the 3-stage split-flow turbo

115   pump (Pfeiffer SplitFlow 310) used for the high vacuum of BSQ, PB and TOF, another

116   turbo pump (Pfeiffer TMH-071-P) was installed to draw air from the SSQ and water

117   vapor from the ion source. A butterfly exhaust throttle valve (MKS T3Bi) was used to

118   control the pumping rate of the newly installed turbo pump (Figure 1), and the pressure of

119   the SSQ can be adjusted by the opening percentage of the valve. In practice, the pressure

120   of drift tube is also actively controlled (see below) and SSQ pressure only needs to be

121   adjusted sporadically.

122   The newly built H_3O^+ ToF-CIMS was deployed on the NOAA WP-3D aircraft in

123   March-April, 2015 as part of the Shale Oil and Natural Gas Nexus (SONGNEX)

124   campaign. During SONGNEX, a total of 19 flights were carried out mainly over oil and

125   gas production basins in the western United States. For the detailed flight strategies, the

126   readers are referred to the SONGNEX website

127   (www.esrl.noaa.gov/csd/projects/songnex).

128   A heated Teflon tube (40 °C) mounted inside a winglet on a window plate was used

129   to transport air into the instrument (Figure S1). Pressure at the downstream end of the

130   inlet was regulated to 180 mbar using a pressure controller. A PEEK capillary was placed

131   between the pressure controller and drift tube to further reduce the pressure from 180

132   mbar to the maintained pressure in the drift tube (2.40±0.01 mbar). During SONGNEX,

133   the 11 cm long drift tube had a drift voltage of 710 V and was heated to 50 °C, which

134   resulted in an E/N ratio (electric field to number density) of 120 Td (1 Td= 10^{-17} V cm^2)

135   inside the drift tube. The flow of the inlet varied from ~500 mL min^{-1} at sea level to ~100

136   mL min^{-1} at 6.5 km of altitude. Background signals of the instrument were determined by

137   passing ambient air for 90 s every 30-40 min through a Platinum catalytic converter

138   heated to 350 °C. In-flight calibrations were performed by adding a small flow (0.5-3.0

139   mL min^{-1}) of a ten-component gas standard (see the list in Table 1) to the inlet flow

140   automatically for 90 s every 1-2 hours (Figure S1). Calibrations were conducted by

141   adding the gas standard flow to either clean air from the catalytic converter or ambient air

142   during SONGNEX. A diffusion cell introduced a small amount of 1,3,5-trichlorobenzene

143   ($C_6H_3Cl_3$) into the instrument continuously to facilitate ToF mass calibration at the high

144   ends of the m/z range. Laboratory experiments show that 1,3,5-trichlorobenzene mainly

145   generates $C_6H_3Cl_3H^+$ (m/z 180.9373, 98.5%) in the instrument, with small contributions

146   from $C_6H_3Cl_3^+$ (m/z 179.9295, 1.0%) and $C_6H_3Cl_2H^+$ (m/z 145.9685, 0.4%). The signals

147   of $C_6H_3Cl_3H^+$ ion were around 2000 cps during the SONGNEX campaign.

148   The axial voltage gradients for SSQ and BSQ were tuned using the Thuner

149   software (Tofwerk AG) by maximizing signals of the protonated product ions of several

150   VOC species (acetone, benzene and isoprene), minimizing VOC signals from charge

151   transfer reactions with O_2^+, and maximizing mass resolution of the TOF analyzer before

152   the campaign. In addition, the effects of turning the RF amplitudes of the SSQ and BSQ

153   were explored manually (see below). The voltage of micro-channel plate (MCP) detector

154   for TOF are determined and set before takeoff for each individual flight by maintaining

155   the single ion signal (SIS) at around 1.8 mV·ns, which effectively prevents mass

156   discrimination as the result of MCP aging (Müller et al., 2014b). The extraction

157   frequency of the TOF was set at 25 kHz, which enables to measure masses up to m/z 500.

158   During SONGNEX, mass spectra were averaged and stored to 10 Hz and were further

159   averaged afterward to 1 Hz for the analysis shown in this paper.

160   ToF data were processed using the Tofware software package (v2.5.1)

161   (www.tofwerk.com/tofware) developed by Tofwerk and Aerodyne Research Inc.

162   (www.aerodyne.com). The detailed procedures of the ToF data processing have been

163   presented in a previous publication (Stark et al., 2015). Post-measurement mass

164   calibrations were conducted using 6-7 isolated masses, including m/z 19.0178 (H_3O^+),

165   m/z 29.9974 (NO^+), m/z 31.9893 (O_2^+), m/z 37.0284 ($H_3O^+(H_2O)$), m/z 55.0390

166   ($H_3O^+(H_2O)_2$), *m/z* 125.9610 ($FeH_5O_4H^+$) and *m/z* 180.9373 ($C_6H_3Cl_3H^+$). Mass

167   calibration of the ToF was accurate within 5-10 ppm for various masses, similar to the

168   results reported for another Aerodyne ToF-CIMS instrument (Lee et al., 2014).

169   Instrument functions (peak shape, peak width and baseline) were derived for each

170   individual flight based on the algorithms shown in Stark et al. (2015). High-resolution

171   peak fitting to the mass spectra were performed using a user defined peak list with

172   masses up to m/z 181.

173   In the orthogonal extraction region of the TOF analyzer, ions of different masses

174   have the same energy but different velocities, and are therefore extracted at different duty

175   cycles (Chernushevich et al., 2001). The Tofware software corrects for this effect using

176   the equation of $I_{corr} = I_{raw} \times \sqrt{\frac{55}{m/z}}$ to a reference mass of *m/z* 55. In this study, all of the

177   signals are reported as the ToF duty cycle corrected signals (I_{corr}), unless otherwise

178   noted.

179   **3. H_3O^+ TOF-CIMS instrument performance**

180   **3.1 Quadrupole ion guides**

181   In addition to hydronium ions (H_3O^+), water clusters are also present in the

182   instrument, including protonated water dimers ($H_3O^+(H_2O)$) and protonated water trimers

183   ($H_3O^+(H_2O)_2$). In standard PTR-MS operation, the product ion signals are normalized to

184   the reagent ion count rates to account for drifts in the ion source. Because the reagent

185   ions in the H_3O^+ ToF-CIMS are so strongly dependent on humidity, the measured cluster

186   ion distribution needs to be understood in detail as it affects the normalization procedure

187   and therefore the measured mixing ratios. As the drift tube in H_3O^+ ToF-CIMS is

188   identical to those in PTR-MS, the cluster distribution and their humidity dependence in

189   the drift tube are expected to be similar as in PTR-MS, which has been understood well

190   and described in detail in de Gouw and Warneke (2007). However, the cluster

191   distribution can be altered in the quadrupole ion guides, because the electric field inside

192   the ion guides is not always the same as that in the drift tube. Thus, the reagent ions and

193   VOC signals as a function of various settings of the quadruple ion guides are investigated

194   here.

195   The signals of the reagent ions as a function of the pressure inside the SSQ are

196   shown in Figure 2. As the SSQ pressure increases from 1.0 mbar to 1.5 mbar, the

197   intensities of all reagent ions increase, indicative of better ion transmission through the

198   SSQ at higher pressures. When the SSQ pressure is higher than 1.5 mbar, the H_3O^+ signal

199   starts to decline slightly and water clusters continue to increase, implying that the reagent

200   ions shift to larger clusters at these SSQ pressures. The ratios of $H_3O^+(H_2O)/H_3O^+$

201   ($R_{37/19}$) increase with the SSQ pressure throughout the range studied here. At higher

202   SSQ pressure, the effective de-clustering ability or E/N ratio is reduced. The $H_3O^+(H_2O)_2$

203   ions account for small a fraction of the reagent ions throughout the explored range of

204   SSQ pressures. The signals of protonated benzene and acetone at constant mixing ratios

205   (2.5 ppb) both increase with higher SSQ pressure, although the increase of benzene

206   signals is small when SSQ pressures go beyond 1.5 mbar. The protonated VOC signals

207   correlate better with H_3O^+ than with $H_3O^+(H_2O)$, suggesting that H_3O^+ ions are the

208   dominant participant in proton-transfer reactions, even though H_3O^+ ions are measured at

209   comparable levels as $H_3O^+(H_2O)$ at high SSQ pressures. Along with this observation, the

210   observed slight reduction of H_3O^+ and disproportionally larger enhancement of

211    $H_3O^+(H_2O)$ with SSQ pressures above 1.5 mbar imply that the transmission of H_3O^+ in

212   the SSQ is significantly lower than that of $H_3O^+(H_2O)$ (and other higher *m/z*). Choosing

213   the optimum SSQ pressure therefore represents a trade-off between higher intensities of

214   the reagent (and VOC) ions and lower signals of water clusters. We have selected to run

215   the instrument with the SSQ pressure at 1.30±0.01 mbar during the SONGNEX

216   campaign.

217   In addition to the SSQ pressure, the signals of reagent ions and VOC product ions

218   were also explored as a function of RF amplitudes for both SSQ and BSQ (Figure S2 and

219   Figure S3). From these experiments, the main findings are: (1) as expected, lower RF

220   amplitudes in the BSQ lead to better transmission for light ions but worse ion focusing

221   (Chernushevich et al., 2001). (2) Ion chemistry needs to be taken into account in the SSQ,

222   for example H_3O^+ declines and $H_3O^+(H_2O)$ increases when RF amplitudes decrease from

223   80 V to 40 V. (3) Variations of VOC signals generally follow the reagent ions, but they

224   are influenced more by poorer focusing at low RF amplitudes, especially for heavier

225   VOC masses. (4) O_2^+ signals and charge transfer products of aromatics increase quickly

226   when RF amplitudes of the SSQ are higher than 80 V, possibly due to discharge in the

227   SSQ (TOF-CIMS manual indicates that discharge happens with >200 V). Based on these

228   results, the RF amplitudes of the SSQ and BSQ were set to 50 V and 350 V, respectively.

229   **3.2 Transmission of reagent ions and their humidity dependence**

230   The humidity of the sampled air affects the distribution of the reagent ions in PTR-

231   MS (de Gouw and Warneke, 2007). Figure 3A shows the reagent ion signals versus water

232   vapor mixing ratios (w) of the sampled air from a laboratory experiment. As expected, the

233    $H_3O^+(H_2O)$ signals increase as the air gets more humidified. The signals of $H_3O^+(H_2O)_2$

234   were small, but increase quickly with humidity. However, there is also an increase of

235   H_3O^+ signals with humidity. Compared to dry air with w=0 g/kg, the H_3O^+ signals are

236   52% higher under the condition with w=22.4 g/kg equivalent to a relative humidity (RH)

237   of 90% at 25 °C. This behavior is in marked contrast to the reported dependence of the

238   reagent ions on humidity in a conventional PTR-MS using ion lenses to transfer ions (de

239   Gouw and Warneke, 2007): in these instruments, H_3O^+ decreases and $H_3O^+(H_2O)$

240   increases with rising humidity and the total intensities of the two reagent ions are

241   relatively stable with humidity with the remaining difference explainable from the

242   difference in detection efficiency between H_3O^+ and $H_3O^+(H_2O)$.

243   The distribution of H_3O^+ and $H_3O^+(H_2O)$ ions exiting the SSQ is determined by

244   the distribution of these same ions entering the SSQ as well as the fragmentation and

245   clustering processes that modify the distribution in the SSQ. At the SSQ pressure used, an

246   individual ion entering the SSQ undergoes many collisions that can add or subtract a

247   ligand molecule. As a result, the transmission efficiency of an reagent ion in the SSQ

248   reflects the averaged transmission efficiencies of ions with m/z 19 and m/z 37 weighed

249   by the time the ion spends as H_3O^+ vs. $H_3O^+(H_2O)$. This issue is qualitatively similar to

250   the measured mobilities of H_3O^+ and $H_3O^+(H_2O)$ observed in the drift tube of PTR-MS

251   (Warneke et al., 2001). The larger H_3O^+ signals at higher humidity in the H_3O^+ ToF-

252   CIMS are the result of the low transmission efficiency of H_3O^+ ions compared to other

253   heavier masses, which has been inferred from the dependence of the reagent ions with

254   SSQ pressures above. The low transmission of H_3O^+ ions is related to the low-mass cut-

255   off of the RF-only quadrupoles (Chernushevich et al., 2001). The strong increase in H_3O^+

256   signal intensity with humidity reflects the fact that while ions may be detected as H_3O^+,

257   they spent a larger fraction of time as $H_3O^+(H_2O)$ in the SSQ at higher humidity and are

258   therefore transferred with a higher average transmission efficiency.

259   The transmission efficiency of H_3O^+ ions relative to $H_3O^+(H_2O)$ is quantified

260   using additional laboratory experiments. Methanol and acetonitrile were introduced into

261   the instrument at such high concentrations that significant fractions of the reagent ions

262   were depleted (Figure S4). Methanol and acetonitrile are used, because their product ion

263   masses (m/z 33 and m/z 42) bracket the mass of $H_3O^+(H_2O)$ ions. We observed more

264   product ions of both methanol (CH_4OH^+, *m/z* 33.0335) and acetonitrile ($C_2H_3NH^+$, *m/z*

265   42.0338) than the summed depletion of H_3O^+ and $H_3O^+(H_2O)$. As the transmission factor

266   of $H_3O^+(H_2O)$ ions should be in between protonated methanol and acetonitrile ions, the

267   ratios between H_3O^+ changes and the changes of the sum of product ions and $H_3O^+(H_2O)$

268   ions in each depletion experiment reflect the ratios of the transmission efficiency between

269   H_3O^+ and $H_3O^+(H_2O)$ ($T_{H_3O^+}/T_{H_3O^+(H_2O)}$). From the scatterplots in Figure S4, the

270    $T_{H_3O^+}/T_{H_3O^+(H_2O)}$ ratios are determined to be in the range of 0.21-0.35 and 0.14-0.25

271   from the experiments with methanol and acetonitrile, respectively (Figure S5). The

272   discrepancies between the estimates from methanol and acetonitrile may come from the

273   differences between the transmission factors of m/z 33 and m/z 42 (Figure S6), and/or

274   small amount of methanol forming methanol-water clusters (see section 3.3). The

275   determined $T_{H_3O^+}/T_{H_3O^+(H_2O)}$ ratios are larger at higher water vapor mixing ratios

276   (Figure 3B, also in Figure S5), in accordance with the expectation of a higher effective

277   transmission efficiency of H_3O^+ ions with increasing humidity discusses above.

278   The relationship of $T_{H_3O^+}/T_{H_3O^+(H_2O)}$ versus water vapor mixing ratios shown in

279   Figure 3B can be used to correct the measured H_3O^+ signals to the same transmission

280   efficiency as $H_3O^+(H_2O)$ (Figure 3C). The corrected H_3O^+ signals exhibit slightly lower

281   signals at higher humidity, which is more similar to the relationship observed in the PTR-

282   MS drift tube (de Gouw and Warneke, 2007). The summed signals of the corrected H_3O^+

283   and measured $H_3O^+(H_2O)$ are also shown in Figure 3C. We see higher total reagent ion

284   signals at increasing humidity. It is clear that H_3O^+ ions dominate the reagent ions in the

285   drift tube throughout the explored humidity range, even though the measured H_3O^+

286   signals are lower than $H_3O^+(H_2O)$ ions at high humidity levels. At a high humidity level

287   (RH=90% at 25 °C, w=22.4 g/kg), $H_3O^+(H_2O)$ ions account for 24-30% of the total

288   reagent ions.

289   Taken together, both the signals of the reagent ions and their transmission

290   efficiency in the instrument exhibit non-linear relationships with humidity. The total

291   reagent ion signals can be derived from the determined $T_{H_3O^+}/T_{H_3O^+(H_2O)}$, but it is

292   associated with significant uncertainties (Figure 3C). A simple equation to derive a

293   parameter with little humidity dependence from reagent ion signals seems to be difficult.

294   Thus, the product ion signals will be normalized to H_3O^+ signals of 10^6 cps to account for

295   drifts in the ion source. Normalization to H_3O^+ signals does not involve any mathematical

296   computation of the reagent ions, which may introduce extra uncertainty.

297   The ratios of $H_3O^+(H_2O)$ ions to H_3O^+ ions ($R_{37/19}$) can be used as a proxy for

298   humidity in PTR-MS (de Gouw et al., 2003a). The dependence of $R_{37/19}$ with water

299   vapor mixing ratios of the sampled air is shown in Figure 3D. We see higher $R_{37/19}$ ratios

300   with increasing humidity from both laboratory experiments and ambient measurements

301   during the SONGNEX, suggesting that $R_{37/19}$ is also a good internal humidity indicator

302   for the instrument. The agreement between laboratory experiments and ambient data is

303   good, considering that the humidity sensors used for laboratory experiments were not

304   cross-calibrated with the sensors on the NOAA WP-3D. The correlation coefficients from

305   laboratory experiments and SONGNEX ambient data are 0.98 and 0.99, respectively,

306   both indicative of tight linear relationship of the data points. The intercept in Figure 3D is

307   the result of excess water vapor entering the drift tube from the ion source. Based on the

308   linear fit to SONGNEX data points in Figure 3D, the $R_{37/19}$ ratio in the instrument is 1.4

309   at a humidity level of RH=90% at 25 °C (or w=22.4 g/kg), which will be used to

310   characterize the instrument response and compare with dry conditions in this study.

311   **3.3 The humidity dependence of VOC sensitivities**

312   *3.3.1   Species without significant dehydration and hydration*

313   A series of laboratory experiments were performed to describe instrument

314   sensitivities of various VOC species as a function of humidity. Figure 4 shows the results

315   for acetone and benzene from one of the experiments. Constant mixing ratios (8.0 ppb in

316   Figure 4) of acetone and benzene were introduced into the instruments and the

317   background subtracted raw signals of protonated product ions of the two compounds

318   were observed at various humidities. As described in the previous section, $R_{37/19}$ is used

319   as the indicator of humidity. Protonated acetone signals increase with rising humidity,

320   whereas protonated benzene signals decline under humidified conditions. The signals of

321   protonated acetone and protonated benzene at the humidity level of $R_{37/19}$=1.4,

322   equivalent to RH=90% at 25 °C, are 111% and 32% of those under dry condition,

323   respectively. The humidity dependencies of these two species are similar to that reported

324   for conventional PTR-MS in many previous studies (Warneke et al., 2001;de Gouw et al.,

325   2003a).

326   The normalized signals of acetone and benzene from the humidity experiments

327   are shown in Figure 4B. As illustrated in the previous section, H_3O^+ signals are 52%

328   higher at $R_{37/19}$=1.4 relative to dry condition. The increase of H_3O^+ signals with

329   humidity is apparently larger than the increase of protonated acetone, which in turn leads

330   to a reduction of the normalized protonated acetone signals with increasing humidity.

331   Because of the low transmission of H_3O^+ ions and clustering/de-clustering effects as

332   described earlier, the normalization to reagent ions leads to a different humidity

333   dependence of the normalized signals in the H_3O^+ ToF-CIMS compared to that in the

334   conventional PTR-MS.

335   The normalized signals at varying humidity levels relative to that at dry condition

336   for acetone, benzene and other VOC species are determined. After attempts using several

337   different fit functions to describe the data points, a double exponential function was

338   found to achieve the best representation of the data. The fitted humidity curves for

339   acetone, benzene and other VOC species are compiled in Figure 5. Generally, a stronger

340   humidity dependence was observed for hydrocarbons than for OVOCs. Comparing the

341   results of the aromatics (benzene, toluene, o-xylene, methylstyrene, 1,2,4-

342   trimethylbenzene and p-cymene), we see less humidity dependence for heavier aromatics.

343   The same trend is also observed for ketones (acetone, MEK, pentanone and hexanone).

344   The heavier species in the two compound series tend to have higher proton affinities (*PA*)

345   (Hunter and Lias, 1998), suggesting that proton affinities of the species play a role in the

346   humidity dependence.

347   The fractions of normalized signals at $R_{37/19}$=1.4 relative to dry condition

348 ($f_{R_{37/19}=1.4}$) were determined and plotted as a function of proton affinities of the species

349 in Figure 5C. A positive correlation between the determined fractions and proton

350 affinities of VOC species is generally observed. This is expected, as a higher proton

351 affinity for a VOC species has several implications: (1) the reaction with $H_3O^+(H_2O)$ ions

352 is exothermic when the proton affinity exceeds that of water dimer (801 kJ/mol); and (2)

353 the reaction more readily becomes exothermic through either direct proton transfer or

354 other routes (Midey et al., 2002). The data points in Figure 5C are color-coded using the

355 permanent dipole moment (μ_D) of the neutrals, which has been shown to affect the

356 efficiency of ligand switching reactions between VOC species and water clusters (Spanel

357 and Smith, 1995). It is clear that species with μ_D<1 D are more strongly humidity

358 dependent than the species with μ_D>1 D, which implies that ligand switching reactions

359 are important in the instrument as the result of substantial amounts of $H_3O^+(H_2O)$ ions.

360 Based on proton affinity and permanent dipole moment, the species shown in Figure 5C

361 can be divided into four groups: group I with PA>801 kJ/mol and μ_D>1 D (e.g. acetone);

362 group II with PA<801 kJ/mol and μ_D>1 D (e.g. acetaldehyde); group III with PA>801

363 kJ/mol and μ_D<1 D (e.g. isoprene); group IV with PA<801 kJ/mol and μ_D<1 D (e.g.

364 benzene). Species in group I (high PA and μ_D) can undergo proton transfer with

365 $H_3O^+(H_2O)$ and H_3O^+ at similar rate constants, whereas the reactions with $H_3O^+(H_2O)$ are

366 either not happening or inefficient for species in group IV (low PA and μ_D). For species

367 in group II (low PA, high μ_D) and III (high PA, low μ_D), ligand switching and direct

368 proton transfer reaction with $H_3O^+(H_2O)$ can occur in the instrument, respectively.

369   The inverse of H_3O^+ signal relative to dry conditions ($\frac{1}{m19}$) was included in Figure

370 5 (A and B) as a reference. If the humidity dependence for a VOC species follows this

371 reference line, the raw signal of the VOC actually has no humidity dependence and the

372 lower normalized signals at higher humidity levels are solely the result of normalization

373 to higher H_3O^+ signals. Species above this reference line are associated with higher raw

374 signals at higher humidity, and vice versa. As discussed in section 3.2, the increase of

375 H_3O^+ signals with rising humidity is caused by a higher effective transmission of ions

376 detected as H_3O^+ (Figure 3B). Thus, the upper limit of the humidity dependence curve

377 should be a flat unity line in Figure 5 (A and B) (see exceptions in section 3.3.2). Many

378   heavier OVOC masses were observed during SONGNEX, but their humidity dependence

379   was not explored. As higher proton affinities are expected for these heavier OVOC

380   species, the humidity dependence curves for these heavier OVOCs should lie in the

381   shaded area filled by patterns in Figure 5 (A and B).

3.3.2   Species with significant dehydration and hydration

383   Product ions of the species explored for humidity dependence in the previous section

384   (3.3.1) are associated with minor dehydration following the proton transfer reaction.

385   Dehydration happens when the product ion of a VOC species fragments by losing one or

386   more water molecules. Propanols and higher alcohols are known to mainly yield

387   dehydration product ions in PTR-MS (Spanel and Smith, 1997;Blake et al.,

388   2009;Warneke et al., 1996). For example, isopropanol (C_3H_7OH, PA=795.4 kJ/mol) is

389   mainly detected as $C_3H_7^+$ (*m/z* 43.0542), rather than $C_3H_8OH^+$ (*m/z* 61.0648) in H_3O^+

390   ToF-CIMS (Figure 6A). We see higher $C_3H_8OH^+/C_3H_7^+$ ratios with increasing humidity

391   in the instrument. The measured humidity dependence of $C_3H_7^+$ ions is similar to that of

392   acetaldehyde (and other OVOCs), whereas more $C_3H_8OH^+$ ions are detected with

393   increasing humidity and the normalized signal of $C_3H_8OH^+$ ions at $R_{37/19}$=1.4 is 1.7

394   times of in dry air. Similar to i-propanol, a positive dependence of protonated ethanol on

395   humidity is also observed (Figure 6B), as ethanol fragments significantly by losing a

396   water molecule as well (Baasandorj et al., 2015).

397   In addition to dehydration, hydrated product ions in the form of $MH^+(H_2O)$ (where

398   M is the formula of VOC species) are observed, including acetaldehyde, acetone,

399   methanol and acetic acid (Figure 7A). The ratios of hydration ions to protonated

400   molecular ions ($MH^+(H_2O)/MH^+$) are observed to increase with humidity for these

401   compounds. Among the species investigated, formic acid (HCOOH, PA=741.8 kJ/mol)

402   and isocyanic acid (HNCO, PA=753.1 kJ/mol) are clustering the most, with

403    $MH^+(H_2O)/MH^+$ ratios of 0.34 and 1.2 at $R_{37/19}$=1.4, respectively. The protonated ions

404   of the two compounds both decrease quickly with humidity, and the normalized signals at

405    $R_{37/19}$=1.4 are both only approximate 2% of those at dry conditions. The signals of

406   hydration ions cannot account for the difference between the humidity dependent curves

407   of these two compounds and the region other OVOCs occupy in Figure 5. The reason for

408   the strong humidity dependence of the two compounds is not known, but it is possibly

409   due to enhanced loss of ions after hydration. A similar enhanced loss of ions at higher

410   humidity was observed for formic acid in a PTR-QMS at a low E/N ratio (85 Td), but not

411   at higher E/N ratios (Baasandorj et al., 2015). Baasandorj et al. (2015) (see Figure 5f in

412   their paper) showed that, at the low E/N ratio (85 Td), protonated ions of formic acid

413   decrease by 12 ncps/ppb and hydration ions only increase by 6 ncps/ppb going from

414   RH=18% to RH=88%. The enhanced loss of isocyanic acid at higher humidity might be

415   related to its hydrolysis, which is reported to be accelerated by water dimer and trimer

416   (Raspoet et al., 1998).

417   The examples of isopropanol, formic acid and isocyanic acid suggest that the

418   humidity dependence can be affected by dehydration and hydration processes of the

419   product ions. The abundance of water molecules affects the equilibrium ratios of the

420   respective ion pairs. In contrast, there are some species associated with significant

421   fragmentation without water molecule as a neutral product, e.g., monoterpenes and p-

422   cymene, which exhibit similar humidity dependence as other VOCs (Figure 5C).

423   Therefore, special attention should be paid to the humidity dependence of the species

424   associated with either significant fragmentation by losing water molecule or significant

425   molecule-water clusters.

426   **3.4 Mass resolving power and separation of isobaric masses**

427   The mass resolving power (m/Δm) was derived from the observed linear

428   relationship between the full-width half maximum (FWHM) of several isolated mass

429   peaks and their *m/z* using Tofware (Stark et al., 2015). The typical m/Δm for the H_3O^+

430   ToF-CIMS during the SONGNEX campaign is shown in Figure S7. The m/Δm in the

431   range of *m/z* 30 - 200 (where most VOCs were detected), are 3900-5900 with higher

432   resolution for heavier masses. These mass resolutions are sufficient to separate many

433   isobaric ions residing at the same nominal masses. Figure 8 shows the separation of C8

434   aromatics ($C_8H_{10}H^+$, *m/z* 107.0855) from benzaldehyde ($C_7H_6OH^+$, *m/z* 107.0491) for *m/z*

435   107 during a flight leg (18:15-18:45 UTC) over the Permian Basin in Texas, US. The two

436   mass spectra in A and B are 30 s averages centered around 18:25:00 and 18:35:10,

437   respectively. The two time windows had either benzaldehyde or C8 aromatics as the

438   higher peak between the two. The time series of benzaldehyde and C8 aromatics

439   determined from the mass spectral fits for this 30-min period correlated well with acetone

440   (*R*=0.87) and benzene (*R*=0.94), respectively. This is consistent with the expectation that

441   benzaldehyde was mainly from secondary formation and C8 aromatics were dominated

442   by primary emissions from oil and gas activities. The signals at *m/z* 107 are usually

443   assigned to C8 aromatics in PTR-QMS studies (de Gouw and Warneke, 2007). Although

444   the possible interference from benzaldehyde to C8 aromatics has been known, it usually

445   constitutes a small fraction of the total signal at nominal mass 107 (Warneke et al., 2003).

446   The example shown in Figure 8 indicates that benzaldehyde, in some environments, can

447   contribute significantly to signals at nominal mass 107.

448   Based on results in previous studies (Stark et al., 2015;Graus et al., 2010), the mass

449   resolving power of the ToF analyzer presented in this study can separate many of the

450   isobaric masses in the mass range of *m/z*<200 by utilizing the high-resolution peak fitting

451   algorithms. The separation of isobaric ions has several advantages over the nominal mass

452   data of PTR-QMS: (1) reduce chemical interferences, e.g. the interference of

453   benzaldehyde to C8 aromatics at nominal *m/z* 107 as shown above; (2) decrease

454   background signals for several compounds of interest, e.g. for methanol (Müller et al.,

455   2014a) and acetaldehyde, the instrument backgrounds of which have interferences from

456   O_2H^+ and CO_2H^+ at the same nominal masses, respectively; (3) increase the number of

457   species that can be measured. In general, 10-20 compounds are usually measurable by the

458   PTR-QMS explicitly without significant interference depending on the origin of the air

459   masses (de Gouw and Warneke, 2007). During the SONGNEX campaign, a total of 1055

460   peaks between *m/z* 12 and *m/z* 181 were identified and assigned to signals in the mass

461   spectra of H_3O^+ ToF-CIMS. Not all of these mass signals can be used for VOC

462   quantification. Many masses (1) are associated with large errors from high-resolution

463   peak fittings as the result of a much larger peak nearby and/or poor separation from

464   another peak; or (2) have no significant enhancement over instrument background. Over

465   260 masses had periods (at least 1 min) with signal to background ratios larger than three

466   during the flight over the Permian Basin on April 23, 2015. Although not all of these

467   masses are attributable to specific compounds, chemical formulas of the masses give

468   more detailed information on the chemical composition than just the nominal *m/z*.

469   Detailed interpretation of the mass spectra in various air masses during the SONGNEX

470   campaign will be presented in a separate publication (Koss et al., in prep).

3.5 Background correction, in-flight calibration and detection limits

471

472   The humidity dependence curves illustrated in Figure 5 were used to correct the

473   normalized signals of various VOC species from measurements made during SONGNEX.

474   After that, background signals were averaged for each measurement cycle and

475   interpolated to the periods between background measurements. Two features in ambient

476   measurements were considered in the interpolation of background signals. First, we

477   observed continuously decrease of background signals for some ions during the flights

478   (Figure S8B). The decrease of background signals cannot be avoided during aircraft

479   measurements, as the instrument only had 2-3 hours start-up time in the morning of each

480   flight day and the instrument backgrounds usually become lower as the instrument runs.

481   Second, background signals for many ions are dependent on humidity in the air, even

482   after the correction for the humidity dependence of their sensitivities (Figure S8D). This

483   is also of particular importance for aircraft measurements, as a rapid change of humidity

484   is encountered during aircraft ascents and descents (de Gouw and Warneke, 2007).

485   Exponential decay function was used to describe the continuous decline of background

486   signals, whereas humidity dependence of background signals was described using linear

487   relationships with one of the humidity indicators ($R_{37/19}$, $H_3O^+(H_2O)_2/H_3O^+$, O_2^+ signals

488   and CO_2^+ signals). Both effects were important for some ions and they were taken into

489   account by consecutive implementation of the procedures (Figure S8C). For other ions, a

490   simple linear interpolation was adopted (Figure S8E). The variations of instrument

491   backgrounds with instrument running time and humidity may also be critical for other

492   PTR-MS and CIMS instruments, especially for aircraft deployments and in some

493   circumstances when meteorological conditions change quickly during ground

494   measurements. The procedures shown here should be easy to incorporate into these

495   measurements if necessary.

496   The measurements of each in-flight calibration are averaged in the same way as the

497   background measurements. The results for benzene, isoprene, acetaldehyde and acetone

498   during the SONGNEX campaign are shown in Figure 9. Each of the four species

499   represents one of the four groups of compounds described in section 3.3. The calibration

500   results for the four species show tight linear correlations between corrected normalized

501   signals and calculated mixing ratios from the gas standard ($R>0.995$), indicating stable

502 instrument performance from flight to flight during the SONGNEX campaign. No clear

503 dependence of sensitivities on $R_{37/19}$ is observed, demonstrating that the effects of

504 humidity on the sensitivities are properly accounted for by the procedures described

505 above. The measured sensitivities for various VOC species are shown in Table 1, which

506 lists sensitivities under dry conditions. The sensitivities for most VOC species of interest

507 are better than 400 cps/ppb, with several species higher than 800 cps/ppb. The lower

508 sensitivity for methanol is consistent with previous studies (Warneke et al., 2015),

509 whereas lower sensitivities for isoprene and α-pinene are due to the fragmentation of their

510 product ions.

511   The counting statistics of the ions follow a Poisson distribution, i.e. the 1-σ error of

512 counting N ions is $\sqrt{N}$. Recent studies showed that the high-resolution peak fitting to the

513 TOF mass spectra can add significant additional noise to the fitted peak intensities of the

514 masses (Cubison and Jimenez, 2015;Corbin et al., 2015). Figure 10 shows standard

515 deviations of the background signals versus the background signals themselves from the

516 individual zeroing periods for the masses listed in Table 1 during one SONGNEX flight

517 (April 27, 2015). Note that the signals shown in Figure 10 were not corrected for the ToF

518 duty cycle, so they represent the actual ion signals detected by the MCP. Real variations

519 of background signals due to instrument drift may contribute some to the standard

520 deviations of background signals. Thus, data points in Figure 10 are best viewed as the

521 upper limits of the errors from counting statistics. Most of the data are observed in the

522 region between $\sqrt{N}$ and $2 \times \sqrt{N}$, suggesting that high-resolution peak fitting can increase

523 the errors in the ion signals by as much as a factor of 2 for the VOC masses in Table 1.

524   The signal to noise ratio (S/N) of the species X from a CIMS instrument can be

525 expressed by (Bertram et al., 2011):

$$\frac{S}{N} = \frac{C_f[X]t}{\alpha \times \sqrt{C_f[X]t + 2Bt}} \qquad (1)$$

526   Here, $[X]$ is the mixing ratios of the species (ppb), C_f is the sensitivity of the species

527 (cps/ppb) and B is the background count (cps), both of which are values without

528 corrections for the ToF duty cycle. t is the sampling time (s). α is the scaling factor of the

529 errors in ion signals relative to Poissonian statistics, and used to account for the

530 additional errors from HR peak fitting. α for each species is determined from Figure 10

531   (see Table 1 for values). We define the detection limit as the mixing ratio with a S/N ratio

532   of 3. The calculated 1-s detection limits for various species are listed in Table 1. The 1-s

533   detection limits are better than 100 ppt for most species. Higher detection limits for

534   acetaldehyde, acetic acid, isoprene, methanol and ethanol are the result of higher

535   background counts for the former two species and lower sensitivities for the latter three

536   species, respectively.

537   Figure 11 compares sensitivities and detection limits of methanol, acetone and

538   benzene between the NOAA PTR-QMS from several previous campaigns (Warneke et

539   al., 2011) and the new H_3O^+ ToF-CIMS during SONGNEX. As discussed in Warneke et

540   al. (2011), the performance of the NOAA PTR-QMS improved gradually as a result of

541   many instrumental developments, which led to higher sensitivities and lower detection

542   limits. As shown in Figure 11, the sensitivity of acetone in the new H_3O^+ ToF-CIMS is

543   similar to that of PTR-QMS in the recent campaigns (CalNex and UBWOS 2013),

544   whereas sensitivities of methanol and acetone are somewhat lower than the PTR-QMS.

545   The performance of a commercial PTR-TOF (PTR-TOF 8000, Ionicon Analytik) during

546   the UBWOS 2013 (Warneke et al., 2015) is also included in Figure 11. We observed

547   much higher sensitivities for our H_3O^+ ToF-CIMS than the PTR-TOF used in UBWOS

548   2013. The large difference in the sensitivities between the PTR-TOF 8000 and H_3O^+

549   ToF-CIMS is mainly attributed to the difference between ion lenses used in the PTR-TOF

550   to transfer ions from the drift tube to the mass analyzer and the quadrupole ion guides

551   used in H_3O^+ TOF-CIMS. A large enhancement in sensitivities of a PTR-TOF by using

552   quadrupole ion guides was recently also demonstrated in a PTR-QiTOF instrument from

553   Ionicon Analytik (Sulzer et al., 2014), which achieved a benzene sensitivity up to 2900

554   cps/ppb.

555   As discussed in the introduction, the operation of a QMS and a TOF-MS is

556   different. The TOF instruments acquire full mass spectra every second (or faster),

557   whereas PTR-QMS is usually operated in selected-ion mode with 1-sec measurement for

558   each of the selected masses every ~15 seconds. So if the total counts measured in each

559   15-second period are calculated (the middle panel in Figure 11), the overall signal to

560   noise of the ToF instruments will compares very favorably to the PTR-QMS.

561   Consistent with the sensitivities, 1-s detection limits of H_3O^+ ToF-CIMS are close

562   to those in PTR-QMS and better than the PTR-TOF used during the UBWOS 2013. As

563   with sensitivities, the detection limits of TOF instruments compare more favorably to

564   QMS if measured data is averaged to the total cycle length of a PTR-QMS to scan the

565   selected masses for their dwell time. We note that the detection limits for methanol,

566   acetone and benzene in the PTR-QiTOF were not reported in Sulzer et al. (2014), and

567   hence a comparison with H_3O^+ ToF-CIMS is not possible at this point.

568   **3.6 Inter-comparisons with GC-MS**

569   In addition to H_3O^+ ToF-CIMS for VOC measurements, whole air samples were

570   collected into canisters in-flight and were analyzed post-flight by GC-MS (iWAS) during

571   the SONGNEX campaign. A total of 72 samples were obtained for most flights. The fill

572   time for each canister was 3-15 s dependent on aircraft altitude. A brief description of the

573   iWAS system was provided in recent publications (de Gouw et al., 2015;Warneke et al.,

574   2016). A few compounds were measured by both H_3O^+ ToF-CIMS and the iWAS

575   system, including benzene, toluene and C8 aromatics. For C8 aromatics, the H_3O^+ ToF-

576   CIMS measured the total mixing ratios of the isomers, whereas the iWAS system was

577   able to measure mixing ratios for the individual isomers (o-xylene, m/p-xylene and

578   ethylbenzene).

579   Figure 12 compares measured results for benzene, toluene and C8 aromatics

580   between H_3O^+ ToF-CIMS and iWAS. The agreement between the two instruments is

581   good for all three aromatic species, with slopes in the range of 0.89-1.1 and correlation

582   coefficients (R) larger than 0.9. We note that there are a few data points with larger

583   disagreement, which are the result of imperfect time alignment of the two measurements

584   during large transient concentration spikes downwind from point sources.

585   **3.7 Applications to ambient measurements**

586   As mentioned above, the H_3O^+ ToF-CIMS was deployed onboard the NOAA WP-

587   3D during the SONGNEX campaign. Figure 13 shows measurement results from a

588   portion of a flight on April 13, 2015 over the Denver-Julesburg Basin, which is an active

589   oil and gas extraction region. Mixing ratios of benzene and toluene were elevated over

590   and downwind from the oil/gas field. Several concentration spikes of the two aromatics

591   were observed and attributed to large point sources related to oil and gas activities. Urban

592   emissions may also contribute to the mixing ratios of benzene and toluene, when the

593   NOAA WP-3D flew over the cities (Loveland, Fort Collins and Greely) in the area. As

594   shown in Figure 13, variations of benzene and toluene mixing ratios below 100 ppt still

595   tracked each other well, illustrating the low detection limits of the two compounds in the

596   H_3O^+ ToF-CIMS. As the emissions of aromatics and other VOCs from motor vehicles are

597   declining in both U.S. and European cities (Warneke et al., 2012;Derwent et al., 2014),

598   the need for techniques (e.g. our H_3O^+ ToF-CIMS) that can measure these compounds

599   rapidly and accurately with low detection limits is increasing.

600   Concentration peaks of acetonitrile were detected several times in this period, when

601   the aircraft sampled plumes from agricultural burns in the area (de Gouw et al., 2003b).

602   The concentration peaks of acetonitrile were pretty narrow, especially the one at 21:34

603   UTC (see the inserted graph in Figure 13B). These small fire plumes can be easily missed

604   if a PTR-QMS had been applied for the detection of acetonitrile, as PTR-QMS has a duty

605   cycle of only a few percent for each individual mass, as shown in the inserted plot in

606   13B. Along with acetonitrile, furan and furfural were also observed in these biomass

607   burning plumes. Furan is a known emission from biomass burning and has been detected

608   in the atmosphere mainly using PTR-MS (de Gouw and Warneke, 2007;Karl et al.,

609   2007). In PTR-QMS, furan cannot be distinguished from isoprene. Its aldehyde

610   derivatives, furfurals, were only measured in a recent laboratory experiment of biomass

611   burning emissions (Stockwell et al., 2015) and in a forest fire plume in the US (Müller et

612   al., 2015) both by PTR-TOF.

613   The third class of compounds shown in Figure 13 is acetaldehyde and acetone.

614   Time series of the two OVOCs were similar to those of benzene and toluene with

615   elevated mixing ratios over and downwind from the oil and gas wells, but they lacked the

616   concentration spikes observed for the aromatics, consistent with secondary formation as

617   their main sources. Acetaldehyde and acetone were also enhanced in the biomass burning

618   plumes.

619   As a final example, acetic acid and ethanol were observed in both oil/gas and

620   biomass burning plumes. Additional peaks of acetic acid and ethanol were detected

621   shortly before and after 21:00 UTC. These enhanced mixing ratios were believed to be

622   the result of emissions from agricultural facilities in this area. Weld County, the main

623   flight area shown in Figure 13, is home to over half million beef and dairy cattle in over

624   100 feedlots facilities. Emissions of acetic acid and ethanol from dairy operations have

625   been reported recently in the Central Valley of California (Gentner et al., 2014).

626   Figure 13 demonstrates that four different groups of VOC species exhibited with

627   distinctly different time series and spatial distributions, as the result of their different

628   sources. The examples in Figure 13 illustrate that the high time resolution dataset from

629   H_3O^+ ToF-CIMS provides important information on characterizations of various air

630   masses in the atmosphere. Along with unique tracers (e.g. acetonitrile for biomass

631   burning), rich information on the chemical signatures will help to identify and separate

632   the contributions of different sources to air mass components in the atmosphere.

633   Measurements of secondary products, in conjunction with primary emissions will be

634   valuable to constrain chemical evolution of gas-phase organic carbon in the atmosphere.

635   **4.   Conclusions**

636   In this study, an aircraft-deployable H_3O^+ ToF-CIMS instrument was developed

637   based on a commercial Aerodyne ToF-CIMS. We characterize the humidity dependence

638   of reagent ions and instrument sensitivities for various VOC species. The new H_3O^+ ToF-

639   CIMS has sensitivities in the range of 100-1000 cps/ppbv for many VOCs of interest and

640   the 1-s detection limits are in the range of 20-500 ppt depending on product ion masses

641   and their instrument backgrounds. The instrument was deployed onboard the NOAA WP-

642   3D research aircraft as part of the SONGNEX campaign in March-April of 2015. The

643   measured mixing ratios for several aromatics from the H_3O^+ ToF-CIMS agreed very well

644   with independent GC measurements from whole air samples. Some initial results from

645   the instrument demonstrate that the H_3O^+ ToF-CIMS dataset will be extremely valuable

646   for the characterization of VOC emissions and photochemistry in the atmosphere.

647   We showed that the low transmission of H_3O^+ ions and secondary ion chemistry

648   inside the SSQ complicates signal normalization and interpretation of the humidity

649   dependence of VOC sensitivities. Further development by removal of the SSQ may

650   ameliorate this issue and is being considered. We also anticipate a further increase in

651   sensitivities from these modifications, as shown in a recent publication (Sulzer et al.,

652   2014). We show that many instrument settings, including SSQ pressure, RF voltages in

653   quadrupoles and the axial voltage gradients along the quadrupoles, affect both reagent

654   ions and VOC signals significantly in our instrument. Some of these effects were

655   explored or seen in other Aerodyne TOF-CIMS instruments as well (Zheng et al.,

656   2015;Lopez-Hilfiker et al., 2015). The next generation of PTR-MS (PTR-QiTOF) that

657   uses quadrupole ion guides for ion transmission may also be affected by some of

658   secondary ion chemistry in the quadrupole. Instruments using different ion chemistry are

659   expected to behave differently with these settings. Therefore, characterization of each

660   individual instrument for these variations and calibrations using authentic standards are

661   essential for generating high quality measurement data with these sophisticated CIMS

662   instruments.

663

664

665

666   *Acknowledgement*

667   We would like to thank Andy Newman for providing the permeation source of

668   formic acid, and Yong Liu and James Roberts for providing the calibration source of

669   isocyanic acid. A. Koss acknowledges support from the NSF Graduate Fellowship

670   Program and the CIRES Graduate Student Research Award. We gratefully acknowledge

671   the support from our colleagues at the NOAA Aircraft Operations Center for help with

672   the installation of the instrument on the NOAA WP-3D and conducting the flights.

673

674
675 **References:**

676 Atkinson, R.: Atmospheric chemistry of VOCs and NOx, Atmospheric Environment, 34,
677   2063-2101, 2000.
678 Baasandorj, M., Millet, D. B., Hu, L., Mitroo, D., and Williams, B. J.: Measuring acetic
679   and formic acid by proton-transfer-reaction mass spectrometry: sensitivity, humidity
680   dependence, and quantifying interferences, Atmospheric Measurement Techniques,
681   8, 1303-1321, 10.5194/amt-8-1303-2015, 2015.
682 Bertram, T. H., Kimmel, J. R., Crisp, T. A., Ryder, O. S., Yatavelli, R. L. N., Thornton, J.
683   A., Cubison, M. J., Gonin, M., and Worsnop, D. R.: A field-deployable, chemical
684   ionization time-of-flight mass spectrometer, Atmos. Meas. Tech., 4, 1471-1479,
685   10.5194/amt-4-1471-2011, 2011.
686 Blake, R. S., Whyte, C., Hughes, C. O., Ellis, A. M., and Monks, P. S.: Demonstration of
687   proton-transfer reaction time-of-flight mass spectrometry for real-time analysis of
688   trace volatile organic compounds, Analytical Chemistry, 76, 3841-3845,
689   10.1021/ac0498260, 2004.
690 Blake, R. S., Monks, P. S., and Ellis, A. M.: Proton-Transfer Reaction Mass
691   Spectrometry, Chemical Reviews, 109, 861-896, Doi 10.1021/Cr800364q, 2009.
692 Chernushevich, I. V., Loboda, A. V., and Thomson, B. A.: An introduction to
693   quadrupole–time-of-flight mass spectrometry, Journal of Mass Spectrometry, 36,
694   849-865, 10.1002/jms.207, 2001.
695 Corbin, J., Othman, A., D. Allan, J., R. Worsnop, D., D. Haskins, J., Sierau, B.,
696   Lohmann, U., and A. Mensah, A.: Peak-fitting and integration imprecision in the
697   Aerodyne aerosol mass spectrometer: effects of mass accuracy on location-
698   constrained fits, Atmospheric Measurement Techniques, 8, 4615-4636, 10.5194/amt-
699   8-4615-2015, 2015.
700 Cubison, M. J., and Jimenez, J. L.: Statistical precision of the intensities retrieved from
701   constrained fitting of overlapping peaks in high-resolution mass spectra,
702   Atmospheric Measurement Techniques, 8, 2333-2345, 10.5194/amt-8-2333-2015,
703   2015.
704 de Gouw, J., and Warneke, C.: Measurements of volatile organic compounds in the
705   earth's atmosphere using proton-transfer-reaction mass spectrometry, Mass
706   Spectrometry Reviews, 26, 223-257, 2007.
707 de Gouw, J. A., Goldan, P. D., Warneke, C., Kuster, W. C., Roberts, J. M., Marchewka,
708   M., Bertman, S. B., Pszenny, A. A. P., and Keene, W. C.: Validation of proton
709   transfer reaction-mass spectrometry (PTR-MS) measurements of gas-phase organic
710   compounds in the atmosphere during the New England Air Quality Study (NEAQS)
711   in 2002, Journal of Geophysical Research-Atmospheres, 108,
712   doi:10.1029/2003JD003863, 10.1029/2003jd003863, 2003a.
713 de Gouw, J. A., Warneke, C., Parrish, D. D., Holloway, J. S., Trainer, M., and
714   Fehsenfeld, F. C.: Emission sources and ocean uptake of acetonitrile (CH3CN) in the
715   atmosphere, Journal of Geophysical Research-Atmospheres, 108,
716   doi:10.1029/2002JD002897, 10.1029/2002jd002897, 2003b.
717 de Gouw, J. A., McKeen, S. A., Aikin, K. C., Brock, C. A., Brown, S. S., Gilman, J. B.,
718   Graus, M., Hanisco, T., Holloway, J. S., Kaiser, J., Keutsch, F. N., Lerner, B. M.,
719   Liao, J., Markovic, M. Z., Middlebrook, A. M., Min, K. E., Neuman, J. A., Nowak, J.

720   B., Peischl, J., Pollack, I. B., Roberts, J. M., Ryerson, T. B., Trainer, M., Veres, P.
721   R., Warneke, C., Welti, A., and Wolfe, G. M.: Airborne measurements of the
722   atmospheric emissions from a fuel ethanol refinery, Journal of Geophysical
723   Research: Atmospheres, 120, 4385-4397, 10.1002/2015jd023138, 2015.
724 Derwent, R. G., Dernie, J. I. R., Dollard, G. J., Dumitrean, P., Mitchell, R. F., Murrells,
725   T. P., Telling, S. P., and Field, R. A.: Twenty years of continuous high time
726   resolution volatile organic compound monitoring in the United Kingdom from 1993
727   to 2012, Atmospheric Environment, 99, 239-247, 10.1016/j.atmosenv.2014.10.001,
728   2014.
729 Ennis, C. J., Reynolds, J. C., Keely, B. J., and Carpenter, L. J.: A hollow cathode proton
730   transfer reaction time of flight mass spectrometer, International Journal of Mass
731   Spectrometry, 247, 72-80, 10.1016/j.ijms.2005.09.008, 2005.
732 Gentner, D. R., Ford, T. B., Guha, A., Boulanger, K., Brioude, J., Angevine, W. M., de
733   Gouw, J. A., Warneke, C., Gilman, J. B., Ryerson, T. B., Peischl, J., Meinardi, S.,
734   Blake, D. R., Atlas, E., Lonneman, W. A., Kleindienst, T. E., Beaver, M. R., Clair, J.
735   M. S., Wennberg, P. O., VandenBoer, T. C., Markovic, M. Z., Murphy, J. G., Harley,
736   R. A., and Goldstein, A. H.: Emissions of organic carbon and methane from
737   petroleum and dairy operations in California's San Joaquin Valley, Atmos. Chem.
738   Phys., 14, 4955-4978, 10.5194/acp-14-4955-2014, 2014.
739 Graus, M., Muller, M., and Hansel, A.: High Resolution PTR-TOF: Quantification and
740   Formula Confirmation of VOC in Real Time, Journal of the American Society for
741   Mass Spectrometry, 21, 1037-1044, DOI 10.1016/j.jasms.2010.02.006, 2010.
742 Hallquist, M., Wenger, J. C., Baltensperger, U., Rudich, Y., Simpson, D., Claeys, M.,
743   Dommen, J., Donahue, N. M., George, C., Goldstein, A. H., Hamilton, J. F.,
744   Herrmann, H., Hoffmann, T., Iinuma, Y., Jang, M., Jenkin, M. E., Jimenez, J. L.,
745   Kiendler-Scharr, A., Maenhaut, W., McFiggans, G., Mentel, T. F., Monod, A.,
746   Prevot, A. S. H., Seinfeld, J. H., Surratt, J. D., Szmigielski, R., and Wildt, J.: The
747   formation, properties and impact of secondary organic aerosol: current and emerging
748   issues, Atmospheric Chemistry and Physics, 9, 5155-5236, 2009.
749 Holzinger, R., Goldstein, A. H., Hayes, P. L., Jimenez, J. L., and Timkovsky, J.:
750   Chemical evolution of organic aerosol in Los Angeles during the CalNex 2010 study,
751   Atmospheric Chemistry and Physics, 13, 10125-10141, 10.5194/acp-13-10125-2013,
752   2013.
753 Hunter, E. P. L., and Lias, S. G.: Evaluated Gas Phase Basicities and Proton Affinities of
754   Molecules: An Update, Journal of Physical and Chemical Reference Data, 27, 413-
755   656, doi:http://dx.doi.org/10.1063/1.556018, 1998.
756 Isaksen, I. S. A., Granier, C., Myhre, G., Berntsen, T. K., Dalsøren, S. B., Gauss, M.,
757   Klimont, Z., Benestad, R., Bousquet, P., Collins, W., Cox, T., Eyring, V., Fowler, D.,
758   Fuzzi, S., Jöckel, P., Laj, P., Lohmann, U., Maione, M., Monks, P., Prevot, A. S. H.,
759   Raes, F., Richter, A., Rognerud, B., Schulz, M., Shindell, D., Stevenson, D. S.,
760   Storelvmo, T., Wang, W. C., van Weele, M., Wild, M., and Wuebbles, D.:
761   Atmospheric composition change: Climate–Chemistry interactions, Atmospheric
762   Environment, 43, 5138-5192, 10.1016/j.atmosenv.2009.08.003, 2009.
763 Jordan, A., Haidacher, S., Hanel, G., Hartungen, E., Mark, L., Seehauser, H.,
764   Schottkowsky, R., Sulzer, P., and Mark, T. D.: A high resolution and high sensitivity
765   proton-transfer-reaction time-of-flight mass spectrometer (PTR-TOF-MS),

766   International Journal of Mass Spectrometry, 286, 122-128, DOI
767   10.1016/j.ijms.2009.07.005, 2009.
768   Karl, T. G., Christian, T. J., Yokelson, R. J., Artaxo, P., Hao, W. M., and Guenther, A.:
769   The Tropical Forest and Fire Emissions Experiment: method evaluation of volatile
770   organic compound emissions measured by PTR-MS, FTIR, and GC from tropical
771   biomass burning, Atmospheric Chemistry and Physics, 7, 5883-5897, 2007.
772   Kaser, L., Karl, T., Schnitzhofer, R., Graus, M., Herdlinger-Blatt, I. S., DiGangi, J. P.,
773   Sive, B., Turnipseed, A., Hornbrook, R. S., Zheng, W., Flocke, F. M., Guenther, A.,
774   Keutsch, F. N., Apel, E., and Hansel, A.: Comparison of different real time VOC
775   measurement techniques in a ponderosa pine forest, Atmos. Chem. Phys., 13, 2893-
776   2906, 10.5194/acp-13-2893-2013, 2013.
777   Lee, B. H., Lopez-Hilfiker, F., Mohr, C., Kurtén, T. C., Worsnop, D., and Thornton, J.
778   A.: An Iodide-Adduct High-Resolution Time-of-Flight Chemical-Ionization Mass
779   Spectrometer: Application to Atmospheric Inorganic and Organic Compounds,
780   Environmental Science & Technology, 10.1021/es500362a, 2014.
781   Lerner, B.: A new analysis system for whole air sampling: description and early results,
782   in prep.
783   Lindinger, W., Hansel, A., and Jordan, A.: On-line monitoring of volatile organic
784   compounds at pptv levels by means of proton-transfer-reaction mass spectrometry
785   (PTR-MS) - Medical applications, food control and environmental research,
786   International Journal of Mass Spectrometry, 173, 191-241, 1998.
787   Lopez-Hilfiker, F. D., Iyer, S., Mohr, C., Lee, B. H., D'Ambro, E. L., Kurtén, T., and
788   Thornton, J. A.: Constraining the sensitivity of iodide adduct chemical ionization
789   mass spectrometry to multifunctional organic molecules using the collision limit and
790   thermodynamic stability of iodide ion adducts, Atmos. Meas. Tech. Discuss., 8,
791   10875-10896, 10.5194/amtd-8-10875-2015, 2015.
792   Midey, A. J., Williams, S., Arnold, S. T., and Viggiano, A. A.: Reactions of
793       $H_3O^+(H_2O)_{0,1}$ with Alkylbenzenes from 298 to 1200 K†, The Journal of Physical
794   Chemistry A, 106, 11726-11738, 10.1021/jp014141e, 2002.
795   Mielke, L. H., Erickson, D. E., McLuckey, S. A., Muller, M., Wisthaler, A., Hansel, A.,
796   and Shepson, P. B.: Development of a Proton-Transfer Reaction-Linear Ion Trap
797   Mass Spectrometer for Quantitative Determination of Volatile Organic Compounds,
798   Analytical Chemistry, 80, 8171-8177, 10.1021/ac801328d, 2008.
799   Müller, M., Graus, M., Ruuskanen, T. M., Schnitzhofer, R., Bamberger, I., Kaser, L.,
800   Titzmann, T., Hörtnagl, L., Wohlfahrt, G., Karl, T., and Hansel, A.: First eddy
801   covariance flux measurements by PTR-TOF, Atmos. Meas. Tech., 3, 387-395,
802   10.5194/amt-3-387-2010, 2010.
803   Müller, M., Mikoviny, T., Feil, S., Haidacher, S., Hanel, G., Hartungen, E., Jordan, A.,
804   Märk, L., Mutschlechner, P., Schottkowsky, R., Sulzer, P., Crawford, J. H., and
805   Wisthaler, A.: A compact PTR-ToF-MS instrument for airborne measurements of
806   volatile organic compounds at high spatiotemporal resolution, Atmos. Meas. Tech.,
807   7, 3763-3772, 10.5194/amt-7-3763-2014, 2014a.
808   Müller, M., Mikoviny, T., and Wisthaler, A.: Detector aging induced mass discrimination
809   and non-linearity effects in PTR-ToF-MS, International Journal of Mass
810   Spectrometry, 365-366, 93-97, 10.1016/j.ijms.2013.12.008, 2014b.

811   Müller, M., Anderson, B., Beyersdorf, A., Crawford, J. H., Diskin, G., Eichler, P., Fried,
812   A., Keutsch, F. N., Mikoviny, T., Thornhill, K. L., Walega, J. G., Weinheimer, A. J.,
813   Yang, M., Yokelson, R., and Wisthaler, A.: In situ measurements and modeling of
814   reactive trace gases in a small biomass burning plume, Atmospheric Chemistry and
815   Physics Discussions, 15, 31501-31536, 10.5194/acpd-15-31501-2015, 2015.
816   Park, J.-H., Goldstein, A. H., Timkovsky, J., Fares, S., Weber, R., Karlik, J., and
817   Holzinger, R.: Active Atmosphere-Ecosystem Exchange of the Vast Majority of
818   Detected Volatile Organic Compounds, Science, 341, 643-647,
819   10.1126/science.1235053, 2013.
820   Raspoet, G., Nguyen, M. T., McGarraghy, M., and Hegarty, A. F.: Experimental and
821   Theoretical Evidence for a Concerted Catalysis by Water Clusters in the Hydrolysis
822   of Isocyanates, The Journal of Organic Chemistry, 63, 6867-6877,
823   10.1021/jo980639+, 1998.
824   Spanel, P., and Smith, D.: Reactions of Hydrated Hydronium Ions and Hydrated
825   Hydroxide Ions with Some Hydrocarbons and Oxygen-Bearing Organic Molecules,
826   The Journal of Physical Chemistry, 99, 15551-15556, 10.1021/j100042a033, 1995.
827   Spanel, P., and Smith, D.: SIFT studies of the reactions of H3O+, NO+ and O-2(+) with a
828   series of alcohols, International Journal of Mass Spectrometry, 167, 375-388, 1997.
829   Stark, H., Yatavelli, R. L. N., Thompson, S. L., Kimmel, J. R., Cubison, M. J., Chhabra,
830   P. S., Canagaratna, M. R., Jayne, J. T., Worsnop, D. R., and Jimenez, J. L.: Methods
831   to extract molecular and bulk chemical information from series of complex mass
832   spectra with limited mass resolution, International Journal of Mass Spectrometry,
833   10.1016/j.ijms.2015.08.011, 2015.
834   Steeghs, M. M. L., Sikkens, C., Crespo, E., Cristescu, S. M., and Harren, F. J. M.:
835   Development of a proton-transfer reaction ion trap mass spectrometer: Online
836   detection and analysis of volatile organic compounds, International Journal of Mass
837   Spectrometry, 262, 16-24, 10.1016/j.ijms.2006.09.031, 2007.
838   Stockwell, C. E., Veres, P. R., Williams, J., and Yokelson, R. J.: Characterization of
839   biomass burning emissions from cooking fires, peat, crop residue, and other fuels
840   with high-resolution proton-transfer-reaction time-of-flight mass spectrometry,
841   Atmos. Chem. Phys., 15, 845-865, 10.5194/acp-15-845-2015, 2015.
842   Sulzer, P., Hartungen, E., Hanel, G., Feil, S., Winkler, K., Mutschlechner, P., Haidacher,
843   S., Schottkowsky, R., Gunsch, D., Seehauser, H., Striednig, M., Jürschik, S., Breiev,
844   K., Lanza, M., Herbig, J., Märk, L., Märk, T. D., and Jordan, A.: A Proton Transfer
845   Reaction-Quadrupole interface Time-Of-Flight Mass Spectrometer (PTR-QiTOF):
846   High speed due to extreme sensitivity, International Journal of Mass Spectrometry,
847   368, 1-5, 10.1016/j.ijms.2014.05.004, 2014.
848   Tanimoto, H., Aoki, N., Inomata, S., Hirokawa, J., and Sadanaga, Y.: Development of a
849   PTR-TOFMS instrument for real-time measurements of volatile organic compounds
850   in air, International Journal of Mass Spectrometry, 263, 1-11,
851   http://dx.doi.org/10.1016/j.ijms.2007.01.009, 2007.
852   Warneke, C., Kuczynski, J., Hansel, A., Jordan, A., Vogel, W., and Lindinger, W.: Proton
853   transfer reaction mass spectrometry (PTR-MS): propanol in human breath, Int J Mass
854   Spectrom, 154, 61-70, http://dx.doi.org/10.1016/0168-1176(96)04369-8, 1996.
855   Warneke, C., van der Veen, C., Luxembourg, S., de Gouw, J. A., and Kok, A.:
856   Measurements of benzene and toluene in ambient air using proton-transfer-reaction

857   mass spectrometry: calibration, humidity dependence, and field intercomparison,
858   International Journal of Mass Spectrometry, 207, 167-182, 2001.
859   Warneke, C., De Gouw, J. A., Kuster, W. C., Goldan, P. D., and Fall, R.: Validation of
860   atmospheric VOC measurements by proton-transfer-reaction mass spectrometry
861   using a gas-chromatographic preseparation method, Environmental Science &
862   Technology, 37, 2494-2501, 10.1021/es026266i, 2003.
863   Warneke, C., Kato, S., De Gouw, J. A., Goldan, P. D., Kuster, W. C., Shao, M., Lovejoy,
864   E. R., Fall, R., and Fehsenfeld, F. C.: Online volatile organic compound
865   measurements using a newly developed proton-transfer ion-trap mass spectrometry
866   instrument during New England Air Quality Study - Intercontinental Transport and
867   Chemical Transformation 2004: Performance, intercomparison, and compound
868   identification, Environmental Science & Technology, 39, 5390-5397,
869   10.1021/es050602o, 2005.
870   Warneke, C., Veres, P., Holloway, J. S., Stutz, J., Tsai, C., Alvarez, S., Rappenglueck, B.,
871   Fehsenfeld, F. C., Graus, M., Gilman, J. B., and de Gouw, J. A.: Airborne
872   formaldehyde measurements using PTR-MS: calibration, humidity dependence,
873   inter-comparison and initial results, Atmos. Meas. Tech., 4, 2345-2358, 10.5194/amt-
874   4-2345-2011, 2011.
875   Warneke, C., de Gouw, J. A., Holloway, J. S., Peischl, J., Ryerson, T. B., Atlas, E.,
876   Blake, D., Trainer, M., and Parrish, D. D.: Multiyear trends in volatile organic
877   compounds in Los Angeles, California: Five decades of decreasing emissions, J.
878   Geophys. Res., 117, D00V17, 10.1029/2012jd017899, 2012.
879   Warneke, C., Veres, P. R., Murphy, S. M., Soltis, J., Field, R. A., Graus, M. G., Koss, A.,
880   Li, S. M., Li, R., Yuan, B., Roberts, J. M., and de Gouw, J. A.: PTR-QMS vs. PTR-
881   TOF comparison in a region with oil and natural gas extraction industry in the Uintah
882   Basin in 2013, Atmos. Meas. Tech., 8, 411-420, 10.5194/amtd-7-6565-2014, 2015.
883   Warneke, C., Trainer, M., de Gouw, J. A., Parrish, D. D., Fahey, D. W., Ravishankara, A.
884   R., Middlebrook, A. M., Brock, C. A., Roberts, J. M., Brown, S. S., Neuman, J. A.,
885   Lerner, B. M., Lack, D., Law, D., Huebler, G., Pollack, I., Sjostedt, S., Ryerson, T.
886   B., Gilman, J. B., Liao, J., Holloway, J., Peischl, J., Nowak, J. B., Aikin, K., Min, K.
887   E., Washenfelder, R. A., Graus, M. G., Richardson, M., Markovic, M. Z., Wagner,
888   N. L., Welti, A., Veres, P. R., Edwards, P., Schwarz, J. P., Gordon, T., Dube, W. P.,
889   McKeen, S., Brioude, J., Ahmadov, R., Bougiatioti, A., Lin, J., Nenes, A., Wolfe, G.
890   M., Hanisco, T. F., Lee, B. H., Lopez-Hilfiker, F. D., Thornton, J. A., Keutsch, F. N.,
891   Kaiser, J., Mao, J., and Hatch, C.: Instrumentation and Measurement Strategy for the
892   NOAA SENEX Aircraft Campaign as Part of the Southeast Atmosphere Study 2013,
893   Atmos. Meas. Tech. Discuss., 2016, 1-39, 10.5194/amt-2015-388, 2016.
894   Zheng, J., Ma, Y., Chen, M. D., Zhang, Q., Wang, L., Khalizov, A. F., Yao, L., Wang, Z.,
895   Wang, X., and Chen, L. X.: Measurement of atmospheric amines and ammonia using
896   the high resolution time-of-flight chemical ionization mass spectrometry,
897   Atmospheric Environment, 102, 249-259, 10.1016/j.atmosenv.2014.12.002, 2015.
898
899
900

Tables

Table 1. Sensitivities and detection limits of H_3O^+ ToF-CIMS for various VOCs species during the SONGNEX campaign

VOC species	Ion Formula	Sensitivity[1]		Background,	α	1-s detection
		ncps/ppb	cps/ppb[2]	cps[2]	value[3]	limit, ppt
Methanol*	CH_4OH^+	81	158	128	1.34	397
Acetonitrile*	$C_2H_3NH^+$	376	822	26	1.33	45
Acetaldehyde*	$C_2H_4OH^+$	289	654	499	1.36	195
Acetone*	$C_3H_6OH^+$	354	916	261	1.28	97
Acetic acid	$C_2H_4O_2H^+$	209	551	660	1.40	283
Furan	$C_4H_4OH^+$	168	470	11	1.26	58
Isoprene*	$C_5H_8H^+$	73	206	26	1.21	162
MVK	$C_4H_6OH^+$	160	454	46	1.24	85
MEK*	$C_4H_8OH^+$	308	886	48	1.21	45
Benzene*	$C_6H_6H^+$	165	493	22	1.48	96
Toluene*	$C_7H_8H^+$	178	579	6	1.39	47
o-xylene*	$C_8H_{10}H^+$	193	673	4	1.49	40
1,2,4-TMB*	$C_9H_{12}H^+$	185	686	3	1.69	45
α-pinene	$C_{10}H_{16}H^+$	67	263	2	1.24	67

[1] Sensitivity under dry condition;

[2] Calculations using H_3O^+ signal at the typical level of 2.5×10^6 cps during the SONGNEX campaign. The signals or sensitivities are not corrected for the ToF duty cycle (see text).

[3] α is the scaling factor of the errors in ion signals relative to Poissonian statistics (Equation 1).

* Stars indicate that the compounds were calibrated in-flight using the ten-component gas standard.

912 **Figures:**
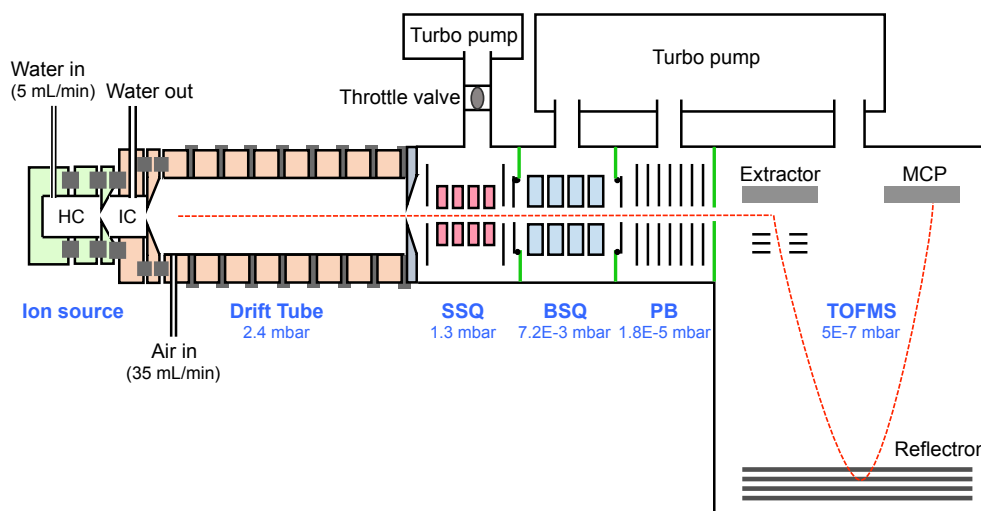
913

914 Figure 1. Schematic drawing of the H_3O^+ ToF-CIMS. HC: hollow-cathode discharge; IC:

915 intermediate chamber; SSQ: small segmented quadrupole; BSQ: big segmented

916 quadrupole; PB: primary beam; MCP: microchannel plate detector.

917
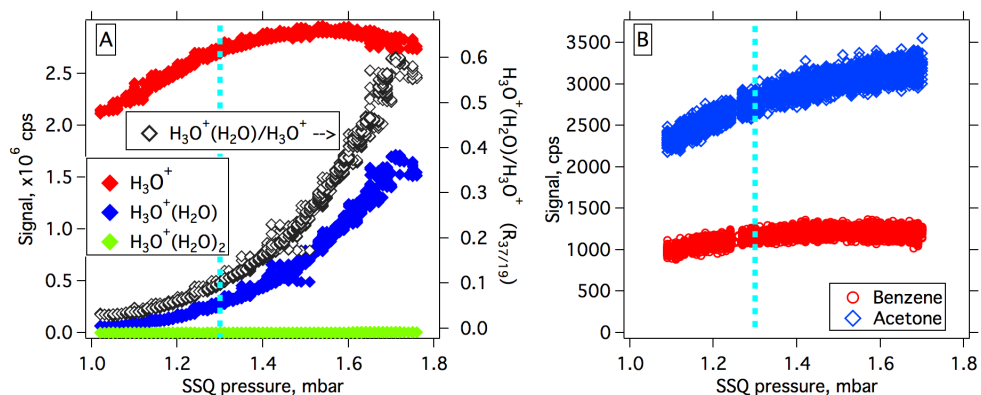
918

919   Figure 2. (A) Signals of reagent ions and $H_3O^+(H_2O)/H_3O^+$ ratio ($R_{37/19}$) as a function of

920   SSQ pressure. (B) Signals of protonated benzene and acetone at constant mixing ratios of

921   2.5 ppb as a function of SSQ pressure. The light blue vertical dashed lines indicate the

922   SSQ pressure (1.30 mbar) used during the SONGNEX campaign.

923

924

925
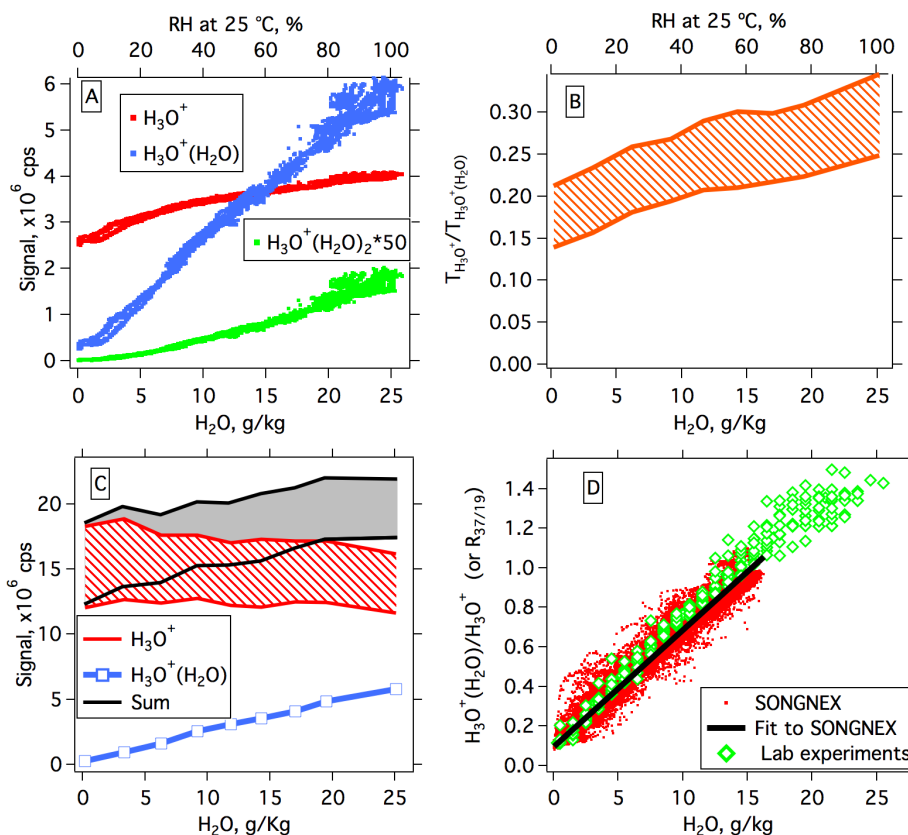
Figure 3. (A) Reagent ion signals as a function of water vapor mixing ratios in the

instrument. (B) Inferred transmission ratios between H_3O^+ and $H_3O^+(H_2O)$ ions

$(T_{H_3O^+}/T_{H_3O^+(H_2O)})$ as a function of water vapor mixing ratios. (C) The H_3O^+ signals and

total signals of the two reagent ions that are corrected to the transmission factor of

$H_3O^+(H_2O)$ ions as a function of water vapor mixing ratios. The measured $H_3O^+(H_2O)$

signals are also shown. The shaded areas in (B) and (C) indicate the possible ranges of

the parameters, which are bounded by estimates from the depletion experiments of

methanol and acetonitrile, respectively. (D) $H_3O^+(H_2O)/H_3O^+$ ($R_{37/19}$) as a function of

water vapor mixing ratios during SONGNEX and from laboratory experiments. The

black line is the linear fit to all of the SONGNEX data.

936

937

938

939

940
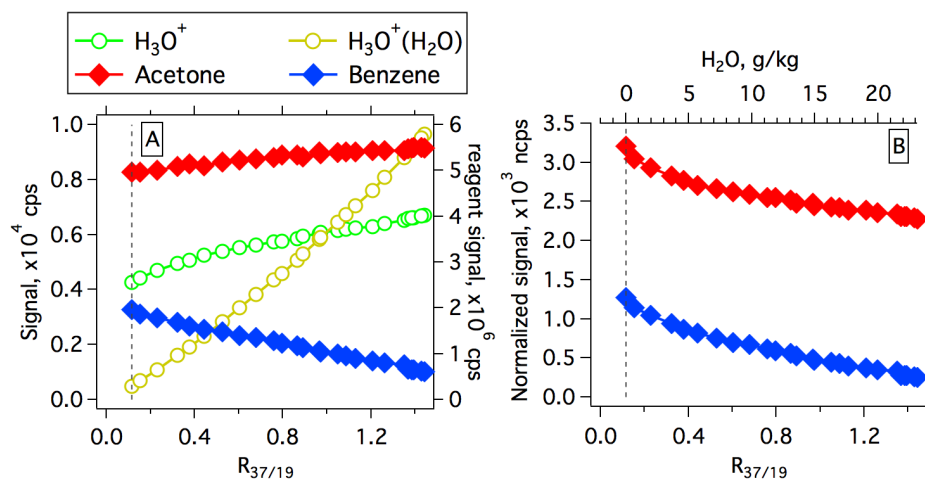
Figure 4. Normalization and humidity dependence of acetone and benzene detection from

a laboratory experiment. (A) Background subtracted raw signals of protonated acetone

and benzene with mixing ratios of 8.0 ppb as the function of $R_{37/19}$. The signals of H_3O^+

and $H_3O^+(H_2O)$ are also shown for reference. (B) Signals of protonated acetone and

benzene normalized to the H_3O^+ signal as a function of $R_{37/19}$.

946

947
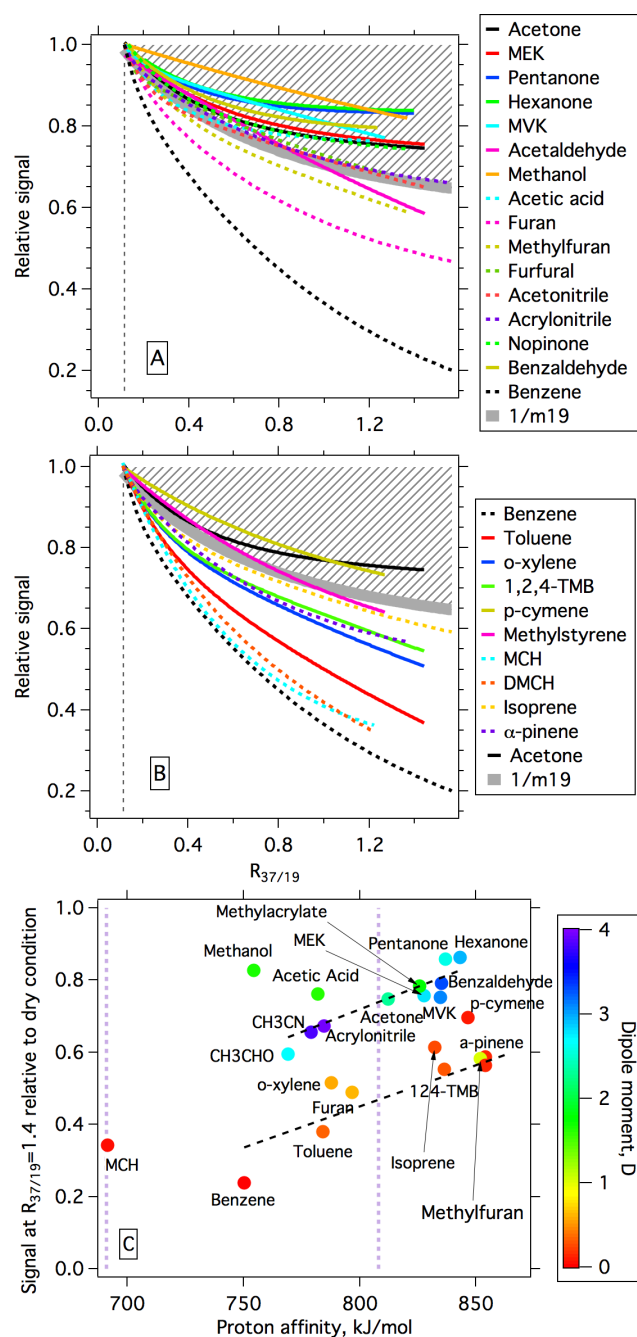
Figure 5. Derived humidity dependence curves for the normalized signals relative to dry
condition as a function of $R_{37/19}$ ratios for oxygenates (A) and hydrocarbons (B),
respectively. The humidity dependent curves of benzene and acetone are shown in both

951 (A) and (B). The thick gray lines indicate the reciprocal of the H_3O^+ signal relative to dry

952 conditions ($\frac{1}{m19}$). Vertical dashed lines in A and B indicate the level of $R_{37/19}$ under dry

953 condition. (C) Normalized signals at $R_{37/19}$=1.4 (equivalent to RH=90% at 25 °C)

954 relative to dry condition for different VOC species as a function of their proton affinities.

955 Data points are color-coded using the permanent dipole moment of the species. The two

956 purple vertical dashed lines are proton affinities of water and water dimer, respectively.

957 The two black dashed lines indicate the linear fits to the species with permanent dipole

958 moment larger than 1 (y=-1.30+2.52×10⁻³×PA) and lower than 1 (y=-1.38+2.29×10⁻³×PA),

959 respectively.

960

961

962
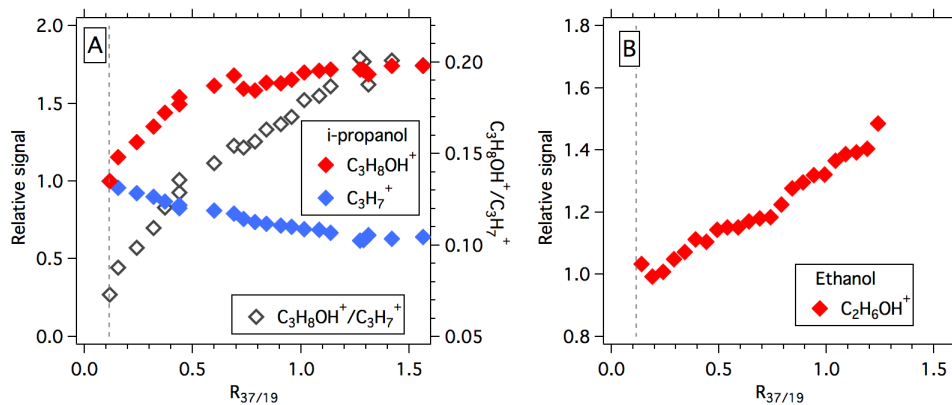
Figure 6. (A) Normalized signals relative to dry condition for protonated and dehydrated ions of isopropanol as a function of $R_{37/19}$ ratios. The vertical dashed line indicates the level of $R_{37/19}$ under dry condition. (B) Normalized signals relative to dry condition for protonated ion of ethanol as a function of $R_{37/19}$ ratios.

967

968
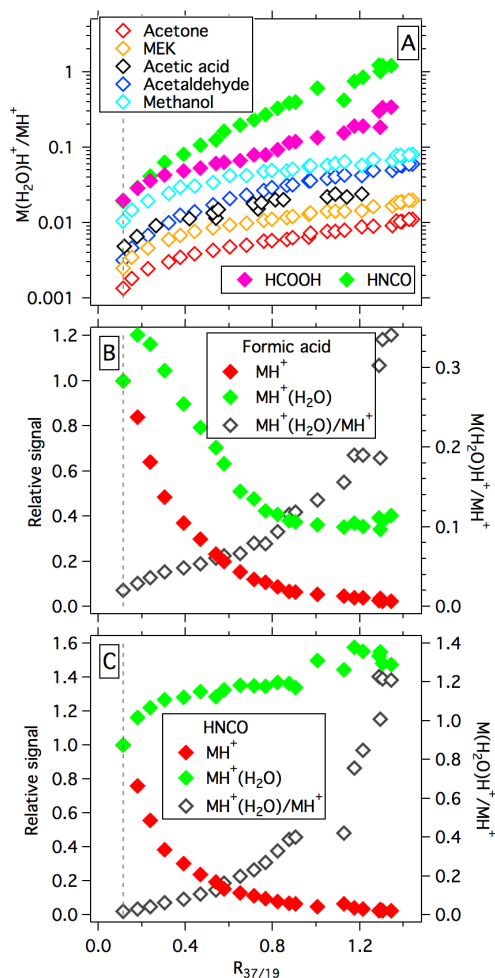
Figure 7. (A) The ratios of hydrated ions to protonated ions for several OVOC species as

a function of $R_{37/19}$ ratios. (B and C) Normalized signals relative to dry condition for

protonated and hydrated ions of formic acid (HCOOH, B) and isocyanic acid (HNCO, C)

as a function of $R_{37/19}$ ratios. The ratios of hydrated ions to protonated ions for formic

acid and isocyanic acid versus $R_{37/19}$ ratios are also shown in (B) and (C), respectively.

Vertical dashed lines in each panel indicate the level of $R_{37/19}$ under dry condition.

975

976

977

978
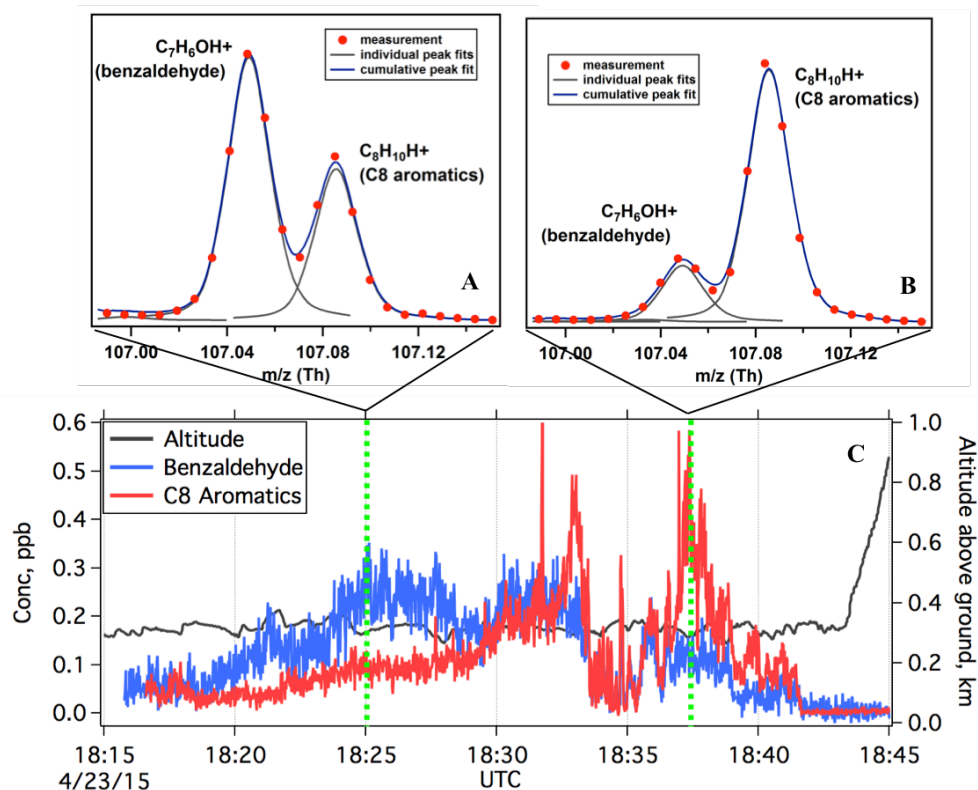
979

980   Figure 8. Separation of benzaldehyde and C8 aromatics from the nominal mass at *m/z*

981   107 in a period (18:15-18:45 UTC) during the flight over the Permian Basin on April 23,

982   2015. (A and B) HR peak fittings of mass spectra at *m/z* 107 at 18:25 and 18:37,

983   respectively. (C) Time series of benzaldehyde and C8 aromatics during the period. Flight

984   altitude of the NOAA WP-3D aircraft is included in C.

985

986

987
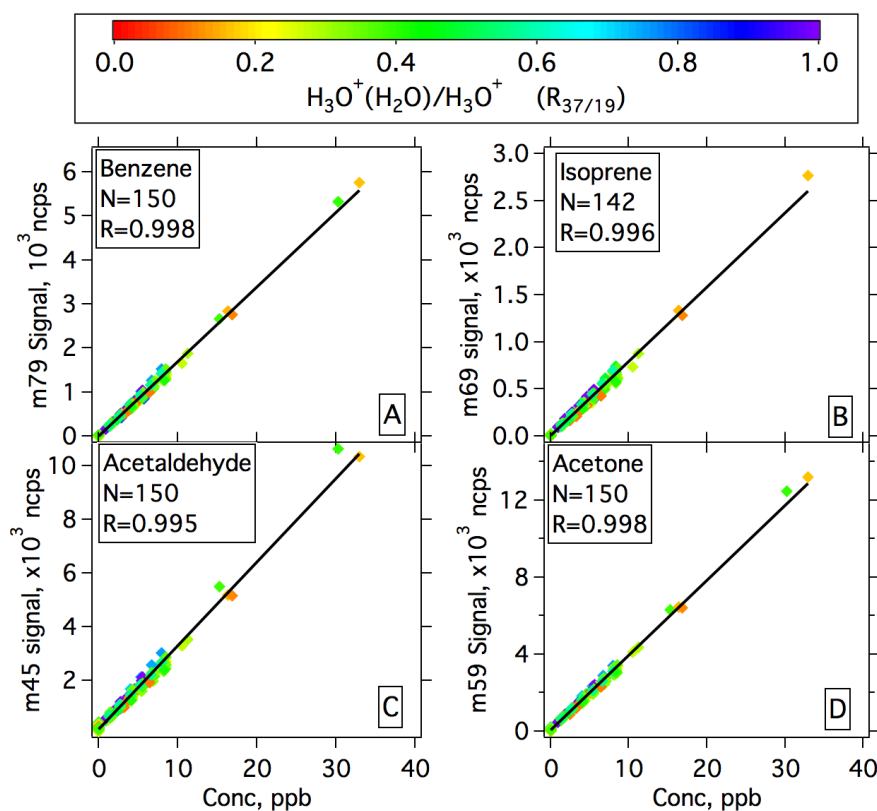
988

989   Figure 9. Inflight calibration results of benzene (A), isoprene (B), acetaldehyde (C) and

990   acetone (D) during the SONGNEX campaign. Signals for the species have been humidity

991   corrected. Data points are color-coded using $R_{37/19}$ ratios. The total times (N) when gas

992   standard was introduced into the instrument during SONGNEX and correlation

993   coefficients (R) are shown in the textbox.

994

995

996
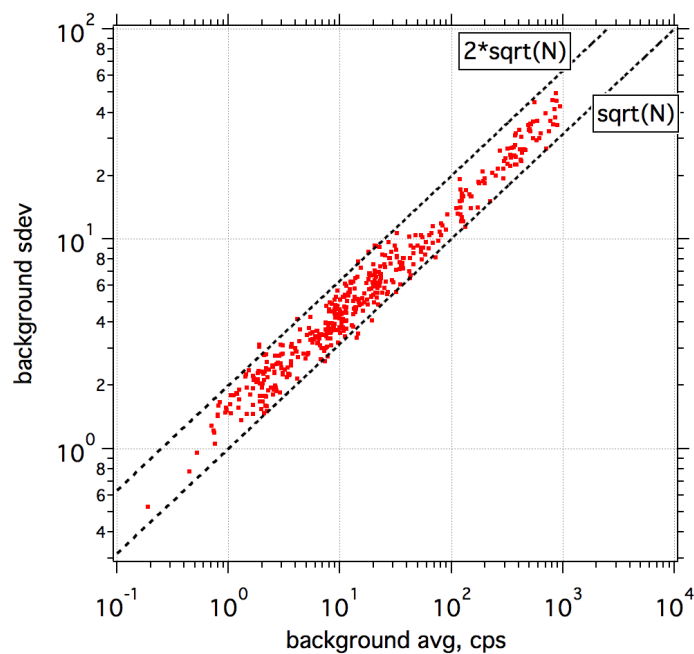
Figure 10. Scatterplot of the standard deviations of background signals versus the measured background signals from a flight on April 27, 2015 during SONGNEX. In this graph, the signals are not corrected for the ToF duty cycle to better reflect the counting statistics of the ToF detector. The two dashed lines are $\sqrt{N}$ and $2\times\sqrt{N}$, respectively.

1001
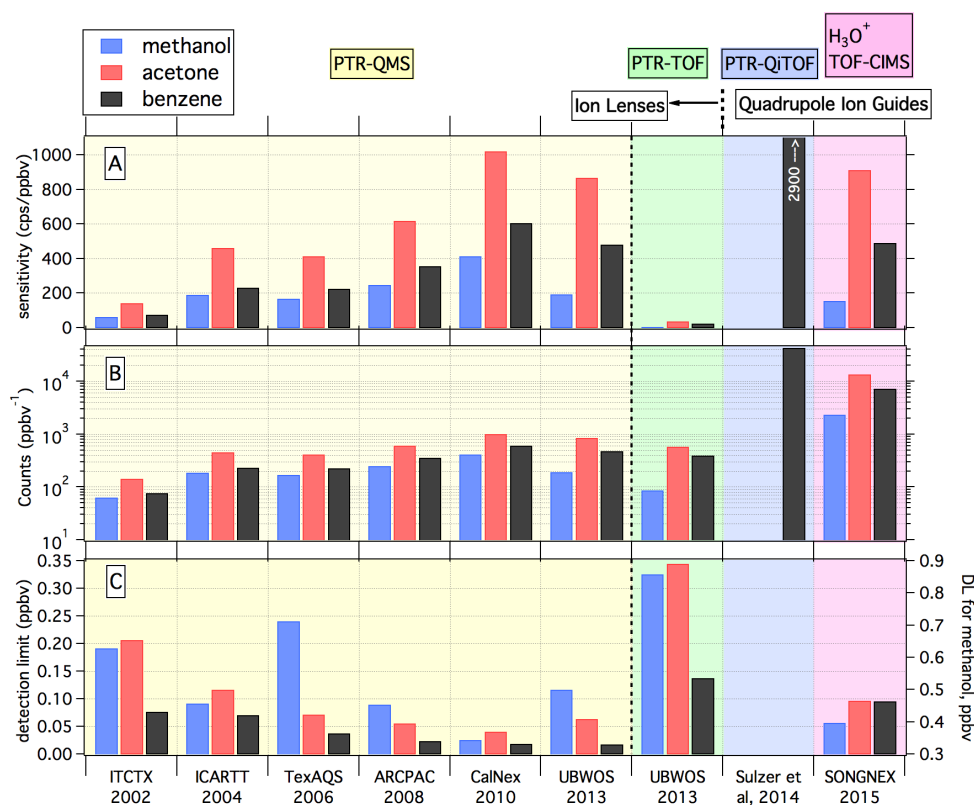
Figure 11. Comparison of the sensitivities (A), total ion counts from measurements in a period of 15 s (B) and 1-s detection limits (C) of methanol, acetone and benzene for the NOAA PTR-QMS (Warneke et al., 2011), a PTR-TOF during UBWOS 2013 (Warneke et al., 2015), the PTR-QiTOF in Sulzer et al. (2014) and the H_3O^+ ToF-CIMS presented here during SONGNEX. In (B), we assume that the PTR-QMS was operated at the typical cycle length of 15 s with 1-s dwell time for the three compounds as have been the norm during our aircraft measurements. Note that the detection limits (DL) of methanol in panel C are drawn on the right axis.
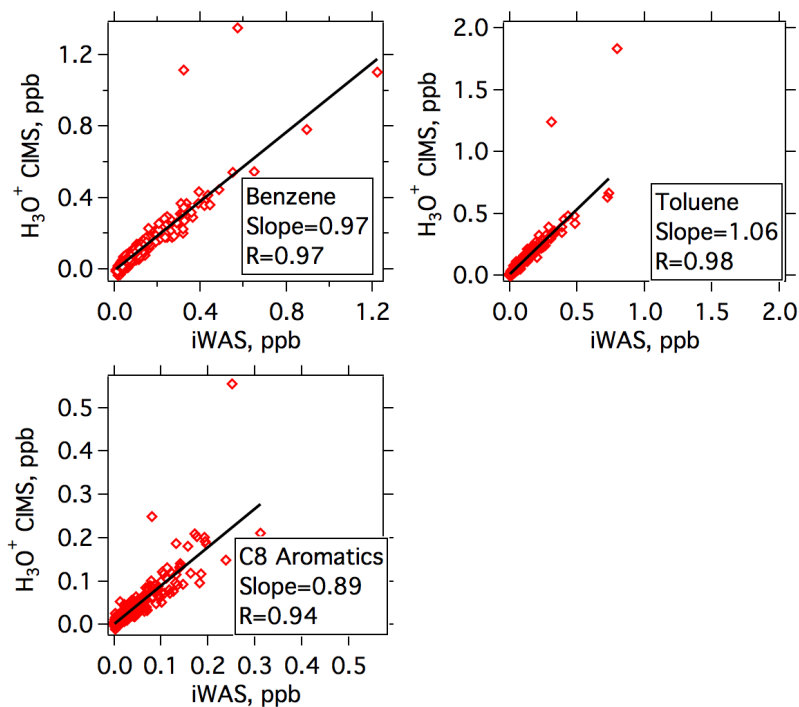
1012

1013 Figure 12. Comparison of measured mixing ratios of benzene, toluene and C8 aromatics

1014 between the H_3O^+ ToF-CIMS and iWAS (Lerner, in prep) during the SONGNEX

1015 campaign.

1016
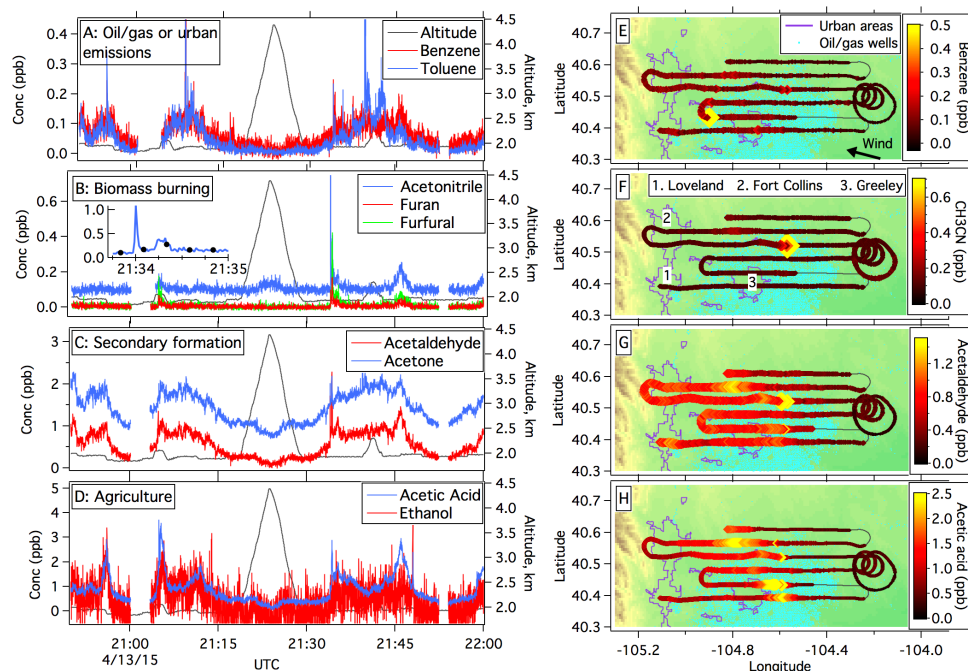
1017

Figure 13. VOC measurements by the H_3O^+ ToF-CIMS for the characterization of air

masses and atmospheric photochemistry during a part of the flight (20:50-22:00 UTC) on

April 13, 2015 over the Denver-Julesburg basin. Time series of various VOC species

from oil/gas or urban emissions (A), biomass burning (B), secondary formation (C) and

agricultural emissions (D) are shown. The inserted plot in B highlights acetonitrile

around 21:34 UTC, where the black dots indicate re-sampled acetonitrile data every 15 s,

reflecting measurement results if a PTR-QMS had been deployed onboard the NOAA

WP-3D. Flight tracks color-coded using mixing ratios of benzene (E), acetonitrile (F),

acetaldehyde (G) and acetic acid (H) are shown in the right panels. Urban regions and

locations of oil and gas wells are indicated in the right panels. The arrow in E indicates

wind direction in the boundary layer during this period.

1029

1030